Earthquake-induced debris flows at Popocatépetl Volcano, Mexico

Velio Coviello[1,2], Lucia Capra[23], Gianluca Norini[34], Norma Dávila[45], Dolors Ferres[56], Víctor Hugo Márquez-Ramirez[23], Eduard Pico[23]

[1] Free University of Bozen-Bolzano, Facoltà di Scienze e Tecnologie, Bolzano, Italy

5 [2] now at Research Institute for Geo-Hydrological Protection, Consiglio Nazionale delle Ricerche, Padova, Italy

[3] Centro de Geociencias, Universidad Nacional Autónoma de México, Campus Juriquilla, Querétaro, México

[4] Istituto di Geologia Ambientale e Geoingegneria, Consiglio Nazionale delle Ricerche, Milano, Italy

[5] Escuela Nacional de Estudios Superiores, Universidad Nacional Autónoma de México, Campus Juriquilla, Querétaro, México

10 [6] Escuela Nacional de Ciencias de la Tierra, Universidad Nacional Autónoma de México, Ciudad de México, México

Correspondence to: Velio Coviello (velio.coviello@unibz.it)

Abstract. The 2017 M_w 7.1 Puebla-Morelos intraslab earthquake (depth = 57 km) severely hit Popocatépetl volcano, ~~volcano flanks,~~ located ~70 km North from the epicenter ~~central Mexico~~. The sSeismic shaking ~~of the volcanic edifice induced by the~~

15 ~~earthquake~~ triggered ~~hundreds of~~ shallow landslides on the volcanic edifice, remobilizing ~~loose pyroclastic deposits and soils~~ slope material saturated by the three-day antecedent rainfall ~~that occurred between 17 and 19 September 2017. The largest landslides occurred on the slopes of aligned ENE-WSW-trending ravines on opposite sides of the volcano, roughly parallel to the regional maximum horizontal stress and local volcanotectonic structural features. This configuration may suggest transient reactivation of local faults and extensional fractures as one of the mechanisms that has weakened the~~

20 ~~volcanic edifice and promoted the largest slope failures. The seismic records from a broadband station located at few kilometers from the main landslides are used to infer the intensity of ground shaking that triggered the slope failures~~. A~~We produced a~~ landslide map ~~was performed~~ based on a semi-automatic classification of a 50-cm resolution optical ~~Placides~~ images acquired two months after the earthquake. We identified Hhundreds of ~~shallow~~ soil slips and three large debris flows ~~were identified,~~ for a total affected area of ~~5~~3.8 km². Landslide distribution appears controlled by the joint effect of slope

25 material properties and topographic amplification. In most ~~of the~~ cases, the ~~slip~~sliding surface~~s~~ correspond~~s~~ with discontinuities between pumice~~-~~fall ~~deposits~~ and massive ash-fall deposit~~s~~ from late Holocene eruptions. The largest landslides occurred on the slopes of aligned ENE-WSW-trending ravines, on opposite sides of the volcano, roughly parallel to the regional maximum horizontal stress and to volcano-tectonic structural features. This suggests transient reactivation of local faults and extensional fractures as one of the mechanisms that has weakened the volcanic edifice and promoted the

30 largest slope failures. The material involved in the larger landslides, ~~mainly ash and pumice fall deposits from late Holocene eruptions with a total volume of about 10⁶ cubic meters,~~ transformed into three large debris flows due to liquefaction, ~~two on the western slope of the volcano and one on its eastern side.~~ The~~se~~ debris flows mobilized a total volume of about 10⁶ cubic meters of material also including large woods, were highly viscous, and ~~contained abundant large woods~~ propagated up to 7.7 km from the initiation areas. We reconstructed this mass wasting cascade by means of ~~Their peculiar rheology is~~

35 ~~reconstructed by~~ field evidences, ~~and grain size distribution of~~ samples from both landslide scarps and deposits, and by analysing remotely sensed and rainfall data. Despite subduction-related earthquakes ~~is~~ are known to produce a smaller number of landslides than shallow crustal earthquakes, the process~~es~~ here described show how an unusual intraslab earthquake can produce an exceptional impact on an active volcano~~, that also determined the co-seismic remobilization of millions of cubic meters of material forming long runout lahars, threating villages at 10 km from the source~~. This scenario,

40 not related to the magmatic activity of the volcano, should be considered in~~for a This is the first time that such flows were observed at this volcano. Our work provides new insights to constrain a~~ multi-hazard risk assessment at Popocatépetl and other active volcanoes located along volcanic arcs.

1 Introduction

Earthquakes can induce large slope instabilities in tectonically active regions, resulting into a relevant source of hazards and

45 damage~~and rainfall events can dramatically increase the sediment load of the drainage network~~. Earthquake magnitude (M) and the resulting intensity of ground vibration control the extent of the area where landslides may occur. One of the first comprehensive historical analysis of earthquake-induced landslides was done by Keefer (1984), who showed that the maximum area likely to be affected by landslides during a seismic event increases with M following a power law scaling relationship. In the following years, a growing number of studies started focusing on the impact of landsliding caused by

50 large-magnitude earthquakes along relatively shallow crustal faults. In particular, it was observed that the fault rupture mechanism ~~can~~strongly influence~~s~~ the distribution of ~~main~~ landslides, which usually are more abundant on the hanging-wall in case of reverse or normal faults (Sato et al., 2007) ~~or~~ and present a symmetric distribution in case of strike-slip faulting (Xu and Xu, 2014). In case of coseismic landslides related to earthquake in subduction-zone, very few data and inventories are available (LaHusen et al., 2020; Schulz et al., 2012; Serey et al., 2019; Wartman et al., 2013). Best example~~s~~ are

55 ~~described for~~ the landslides induced by the 2010 Chile megathrust earthquake (Serey et al., 2019) and by the 2011 Tohoku Earthquake, Japan (Wartman et al., 2013)~~, with peak acceleration rate up to 1g~~. In both cases, thousand~~s~~ of shallow landslides were identified, but the main conclusion ~~from~~of these works ~~suggest~~is that the number of landslides generated by megathrust earthquakes is ~~lower~~smaller than the number of events triggered by shallow crustal earthquakes by at least one or two orders of magnitude. Today, we know that the ~~S~~spatial distribution of earthquake-induced landslide is also a function of

60 geological parameters ~~source material~~ (e.g., contrast in rock coherence, permeability), topography (slope and shape), land-cover and land-use, and ground-motion characteristics such as amplification and shaking frequency (Fan et al., 2019; Von Specht et al., 2019). Concerning the impact of earthquake on sediment-related hazards~~h~~, a dramatic increase of sediment yield has been documented after large earthquake-induced landslides ~~is still an importan process during landsliding~~(Pearce and Watson, 1986; Dadson et al., 2004; Marc et al., 2019). Progressively, source areas on highlands can become quickly

65 stable as fine material is removed ~~or~~and new vegetation grow and stabilize the slope (Domènech et al., 2019) but debris flows can still occur due to remobilization of deposited material along the channel (Fan et al., 2021).

On active volcanoes, a large variety of factors can promote slope instability and failure such as magma intrusions, hydrothermal activity, gravitational spreading of the basements, climate fluctuations and regional tectonic (Capra et al., 2013; Mcguire, 1996; Norini et al., 2008; Roberti et al., 2017; Roverato et al., 2015). In particular, earthquakes are

70 recognized to play one of the most important role in the initiation of slope failures on volcanoes (Kameda et al., 2019; Sassa, 2005; Siebert, 2002). Volcanic slopes that are close to a critical state can be particularly susceptible to perturbations produced by regional earthquakes. Volcanic landslides include a wide spectrum of instability phenomena, from small slope failures to large sector collapse evolving into catastrophic debris avalanches. Intermediate processes such as shallow landslides and debris flows are common in case of an earthquake, but they are relatively poorly documented for past events.

75 Debris flows, often called lahar in volcanic environments, are usually associated with eruptions that induce ice/snow-melt or with intense rainfalls occurring during intra-eruptive phases (e.g., Capra et al., 2018; Major et al., 2016; Manville et al., 2009). Few examples of long-runout debris flows triggered by earthquakes have been described on active volcanoes (Schuster et al., 1996; Scott et al., 2001). In Mexico, a M6.5 earthquake that occurred in 1920 induced several landslides in the Pico de Orizaba - Cofre de Perote volcanic chain that transformed into debris flows with catastrophic effects for villages

80 along the Huizilapan ravine (Camacho, 1920; Flores, 1922). More recently, several thousands of shallow landslides were triggered by the Tecomán earthquake of 21 January 2003 (M 7.6) in the volcanic highlands north and northwest of Colima City (Keefer et al., 2006).

In this paper, we investigate the exceptional mass wasting episode triggered by the 19 September 2017, M_W 7.1 Puebla-Morelos intraslab earthquake along the eastern and western sides of Popocatépetl volcano. The seismic shaking mobilized~~A~~

85 ~~volume of about 10⁶ cubic meters of~~ pre-existing ash and pumice fall deposits ~~have been remobilized,~~ producing hundreds of coseismic soil slips. ~~, t~~The largest ones had a total volume of about 10^6 cubic meters and ~~that~~ transformed into debris flows that traveled ~~more than~~up to 7.7 km on the Western side of the volcanic edifice. This phenomenon, never studied before at Popocatépetl volcano, and probably unique on an active stratovolcano along a continental volcanic arc, has important implications for hazard assessment, as the actual hazard map only includes ~~only~~ the impact of lahars related to volcanic

90 activity (Martin Del Pozzo et al., 2017). ~~Popocatépetl is one of the most active volcanoes in North America and represents a serious threat for infrastructures and human settlements in central Mexico (Figure 1a). The three major late Holocene eruptions produced pumice fall deposits on the north-east and east sides of the volcano with post-eruptive lahars reaching runout distances up to 50 km in the east and south drainages (Siebe et al., 1996). In recent time, only two large lahar events were observed along the Huiloac Gorge (HG, Figure 1b), in 1997 and 2001, associated with eruptive phases (Capra et al.,~~

95 ~~2004). Both lahars propagated to the town of Santiago Xalitzinta, 15 km from the volcano summit (SX, Figure 1b). Apart from the Huiloac Gorge, which was characterized by significant geomorphic transformations due to these latter processes (Tanarro et al., 2010), most drainage network of Popocatépetl volcano has a dense vegetation cover and presents stable, low-energy sediment transport conditions (Castillo et al., 2015). These stable conditions suddenly changed during the M_W 7.1 Puebla-Morelos earthquake when seismic shaking severely hit central Mexico and triggered hundreds of landslides on the~~

100 ~~slopes of Popocatépetl volcano.~~ In the following, we provide a general introduction to the geomorphology of Popocatépetl

volcano and ~~we shortly describe~~to its recent volcanic activity. Then, we describe the impact of the M_w 7.1 Puebla-Morelos earthquake on the volcano slopes in terms of ground vibrations and landslide activity. Finally, we reconstruct the transformation ~~dynamics~~ of the major landslides ~~and we discuss their transformation~~ into long runout debris flows~~,~~ and we discuss the~~ir~~ hazards implication for an active volcano.

2 Background

2.1 Popocatéptl volcano

Popocatépetl volcano (19°03'N, 98°35'W; elevation 5,450 m a.s.l.) is located in the central sector of the Trans-Mexican Volcanic Belt (TMVB) and it represents the active and southernmost stratovolcano belonging to the Sierra Nevada volcanic chain ~~along with the Telapón-Tlalóc-Iztaccíhuatl volcanoes~~ (Pasquaré et al., 1987) (Figure 1a, -b). The Popocatépetl is a composite volcano and its present shape is the result of eruptive activity that rebuilt the modern cone after the 23.5 ka flank collapse (Siebe et al., 2017). During the Last Glacial Maximum (20-14 ka) the glacier activity resulted in extensive moraines and glacial cirques (Vázquez-Selem and Heine, 2011). The lower part of the cone features a gentle slope (10-15°) and a dense vegetation cover up to approximately 3800 m a.s.l. (**Error! Reference source not found.**a), where pine trees became scattered and surrounded by dense tropical alpine grasslands (*zacatonal alpino*, Almeida et al., 1994), that can measure up to 1 m in height. Then, the cone becomes progressively steeper (20-30°) and unvegetated up to the summit ~~(Figure 2)~~. In the upper portion of the cone, the slopes are covered by abundant unconsolidated ash named "~~los~~Los ~~arenales~~Arenales" from the recent vulcanian eruptions (**Error! Reference source not found.**a).

Quaternary ~~Historical~~ volcanic activity of Popocatépetl volcano has been characterized by catastrophic episodes including sector collapses and Plinian eruptions that emplaced pyroclastic density currents and thick pumice fall deposits, predominantly toward the east and northeast (Figure 1b) (Siebe and Macías, 2006). Based on its Holocene eruptive record, Plinian eruptions at Popocatépetl have occurred with variable recurrence time of about 1~~,000~~-3~~,000 years~~ka (Siebe et al., 1996). Since 1994, the volcano entered in a new eruptive phase, which includes domes growth that are subsequently destroyed during strong vulcanian eruptions with columns up to 8 km in height, accompanied with ash fall that have been affecting populations in a radius of 100 km approximately. Eruptive activity played the primary role in accelerating the glacier retreat on the northern slope of the volcano (Julio-Miranda et al., 2008).
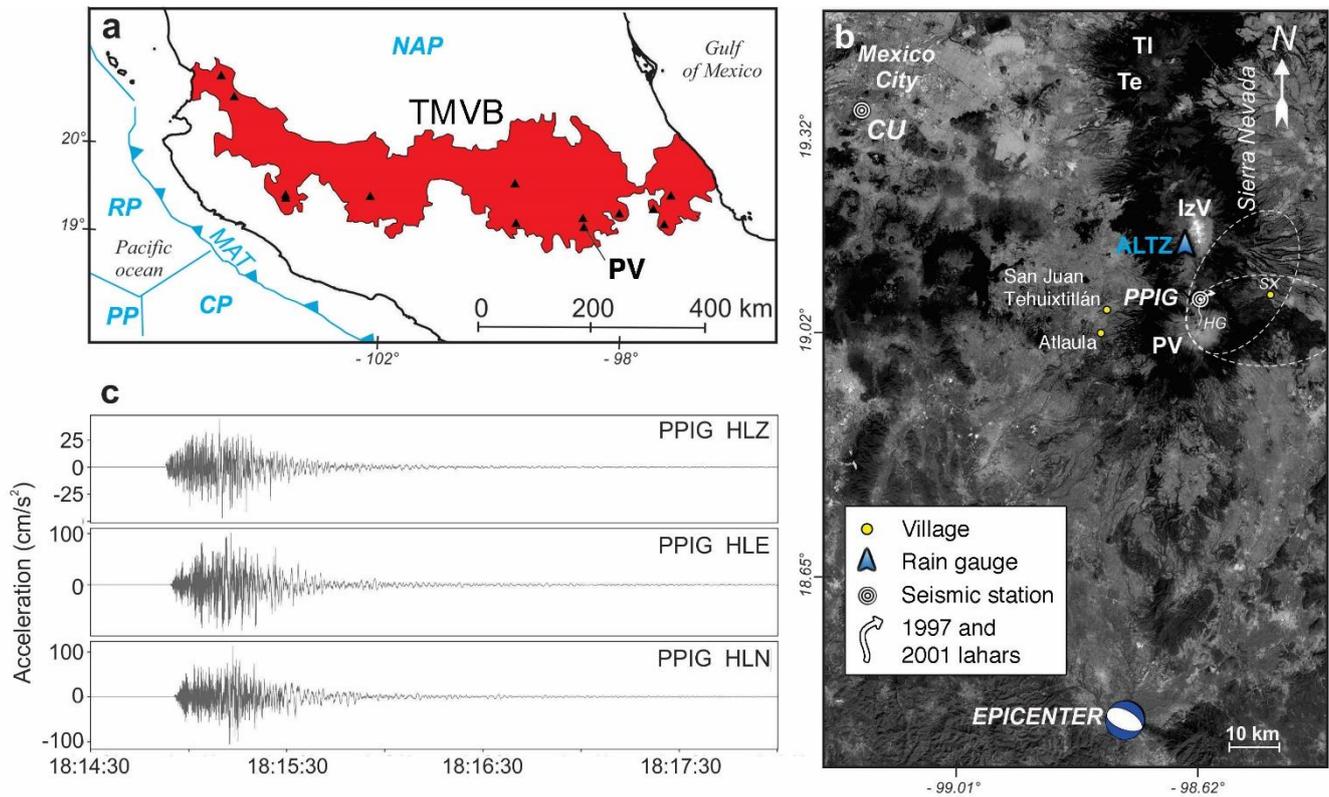
Figure 1: (a) Plate tectonic settings of Central Mexico (CP Cocos Plate, ~~MAT Middle American Trench~~, NAP North America Plate, RP Rivera Plate, PP Pacific Plate, MAT Middle American Trench) and location of Popocatépetl volcano (PV) in the Trans-Mexican Volcanic Belt (TMVB). (b) Details of the area affected by the M_w 7.1 Puebla-Morelos earthquake and location of the seismic station CU and PPIG and of the rain gauge ALTZ. Popocatépetl volcano (PV) is the southernmost edifice of the Sierra Nevada volcanic chain along with the Iztaccihuatl (IzV), Telapón (Te) and Tláloc (Tl) volcanoes. The main distribution areas of the pumice fall deposits from the last two Plinian eruptions of the ~~V~~PV are indicated with white dashed lines (background image Landsat/Copernicus from Google Earth: ©Google 2020, ©INEGI 2020). (c) Strong motion recorded at station PPIG (SSN-UNAM) during the Puebla-Morelos earthquake on ~~17~~ 19 September 2017.

In recent time, only two large lahar events were observed along the Huiloac Gorge (~~HG~~Hg, Figure 1b), in 1997 and 2001, associated with eruptive phases (Capra et al., 2004). At those times, ~~Last major lahars occurred when~~ the Ventorillo glacier was still present on the northern face of the volcano. Both lahars propagated to the town of Santiago Xalitzinta (SX, Figure 1b), located ~15 km E from the volcano's summit. The 1997 lahar originated after a prolonged explosive activity with emission of ash, which caused the partial melt of the glacier. The rapid release of water gradually eroded the river bed and triggered a debris flow. The 2001 lahar originated from the remobilization of a pumice flow deposit emplaced over the Ventorillo glacier on the northern side of the volcano. The event occurred ~5 hrs after the pyroclastic flow emplacement, and the debris flow was characterized by a stable sediment concentration of 0.75 (Capra et al., 2004). In the distal part, the 1997 lahar transformed into a hyperconcentrated flow, while the 2001 one maintained the characteristics of a debris flow~~,~~ due to its apparent cohesion ~~due to~~conferred by a silty-rich matrix inherited from the pumice flow deposit. Apart from the Huiloac

Gorge, which was characterized by significant geomorphic transformations due to these latter processes (Tanarro et al., 2010), most drainage network of Popocatépetl volcano has a dense vegetation cover and presents stable, low-energy sediment transport conditions (Castillo et al., 2015). These stable conditions suddenly changed during the M_W 7.1 Puebla-Morelos earthquake.

2.2 The M_W 7.1 intraslab Puebla-Morelos earthquake

On 19 September 2017, central Mexico was hit by a M_W 7.1 intraslab seismic event (depth = 57 km) named Puebla-Morelos earthquake (Melgar et al., 2018; Singh et al., 2018). The epicenter of this earthquake is was located at a distance of ~about 70 km South from the summit of Popocatépetl volcano and ~of about 100 km South from Mexico City (Figure 1b) with a depth of 57 km. The focal mechanism corresponds to a normal fault with a dip angle of 44°-47° 112°/46° in strike and dip direction (Melgar et al., 2018). The 2017 M_W 7.1 Puebla-Morelos earthquake produced the most intense ground shaking ever recorded in Mexico City during a subduction-related earthquake, and was the most damaging event for this densely urbanized part of the country since the 1985 M_W 8.1 Michoacán interplate earthquake, that occurred exactly 32 years before (Singh et al., 2018). The damage was surprisingly large in the critical frequency range for Mexico City (0.4–1 Hz), where the earthquake severely damaged hundreds of buildings and killed 369 people (Singh et al., 2018). The 2017 intraslab earthquake occurred closer to Mexico City, at greater depth, and involved higher stress drop than their interplate counterparts, such as the 1985 Michoacán event. The stress drop of intraslab events have been estimated as ~4 times greater than that of the interplate earthquakes (García et al., 2005) and. the ground acceleration of the intraslab earthquakes are expected to be more enriched at higher frequencies than those of the interplate events (Furumura and Singh, 2002; Singh et al., 2018). The Peak Ground Acceleration (PGA), calculated as the quadratic mean of the maximum acceleration on the horizontal components, is a standard parameter describing the intensity of strong ground motion during an earthquake. During the 2017 M_W 7.1 Puebla-Morelos earthquake, the Peak Ground Acceleration (PGA) recorded at station Ciudad Universitaria (CU) was the highest recorded in the last 54 years of observations (57.1 cm/s^2) (Singh et al., 2018). Station CU is located on the external boundary of the sedimentary basin responsible for the well-known seismic amplification at Mexico City (Figure 1b). The seismic signal recorded at PPIG station (Figure 1c), located at 3980 m a.s.l. on Popocatépetl volcano slopes at 3980 m a.s.l., featured a much higher value of PGA (106.83 158.16 cm/s^2, 0.1g) than the one observed at station CU.

3 Data and methods

We adopted a combined field- and remote-based approach to retrieve timely and original information about the earthquake impact on such a harsh environment. Semi-automated satellite-image classification is a rapidly developing tool producing reliable landslide sizes maps (e.g., Fan et al., 2019 and references therein). We used Satellite optical satellite data were used

to ~~define the extension of~~identify the _main_ areas affected by landslides and _to constrain_ the timing of the landslide occurrences _with_ respect to the earthquake event _(Figure 2a, b)._ _We constructed Aa_ preliminary landslide map (Figure 2c)

180 ~~was constructed~~ based on the interpretation of an archive Pléiades 1A image (incidence angle of 14.63°, resolution of 0.5 m) acquired two months after the earthquake. A Normalized Difference Vegetation Index (NDVI) was calculated using band 1 (red) and band 4 (infrared). The resulting raster was classified for excluding vegetation cover, roads and buildings from the analysis and selecting only landslide scars or depositional areas ~~(Figure 2)~~. _The final map_ (Figure 2c) _was validated and refined based on field data_ ~~that we collected in the field~~. Most landslides are located on the W side, on the E side, and on the

185 SE side of the volcanic edifice (Figure 3).
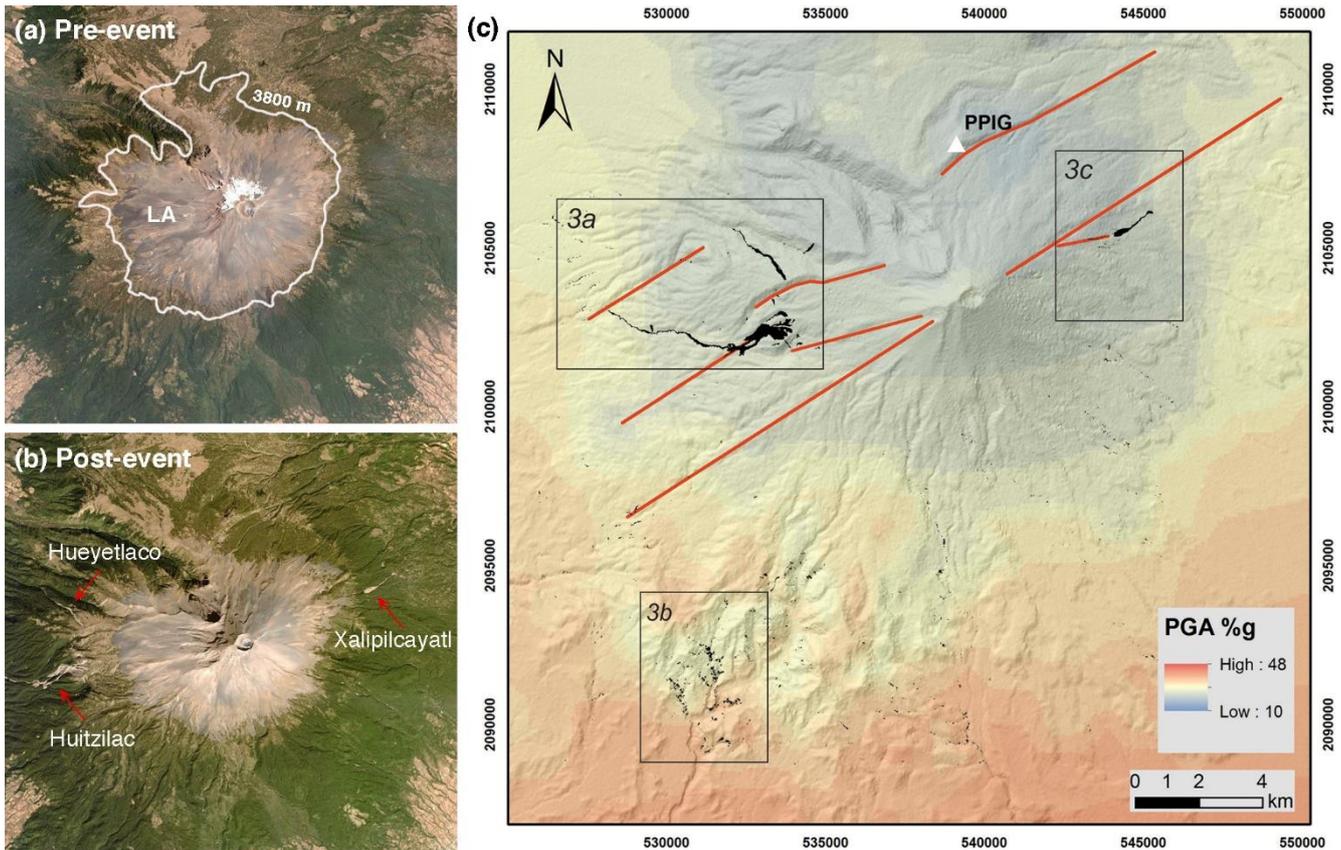
Figure 2: _Optical images of Popocatépetl volcano acquired before and after the M_W 7.1 Puebla-Morelos earthquake (images ©DigitalGlobe) and landslide map. (a) In the pre-event image (acquired on 23 March 2017), the 3800-m line and Los Arenales (LA)_

190 _deposits are indicated in white. (b) In the post-event image (acquired on 11 December 2017), the red arrows indicate the debris flows that occurred in Hutzilac, Hueyatlaco and Xalipilcayatl ravines._ ~~Landslide map of the Popocatépetl volcano after the M_w 7.1 Puebla-Morelos earthquake.~~ _In the landslide map,_ ~~The~~ _the black_ polygons corresponding to landslide scars ~~or~~ _and_ deposits ~~(red areas) or long-runout debris flows (blue areas~~_dashed lines)_ were extracted ~~through the interpretation of~~_from_ a Pléiades 1A image acquired on 13 November 2017. Main volcano-tectonic lineaments are reported _in the map_ (~~brown blackred~~ lines). ~~The black dashed circle contains the cluster of small soil slips~~

195 ~~that occurred on the southwestern side of the volcano.~~ _The white triangle indicates the PPIG seismic station where a PGA of 106.83 cm/s²_ _was measured (Figure 1c)._ The black squares indicate the ~~location of the zoomed~~ areas _zoomed_ in Figure ~~4~~3_._ _Background: map of the PGA distribution (data source: USGS Earthquake Hazard Program) and_ 12.5m DEM ©JAXA/METI ALOS PALSAR 2008.
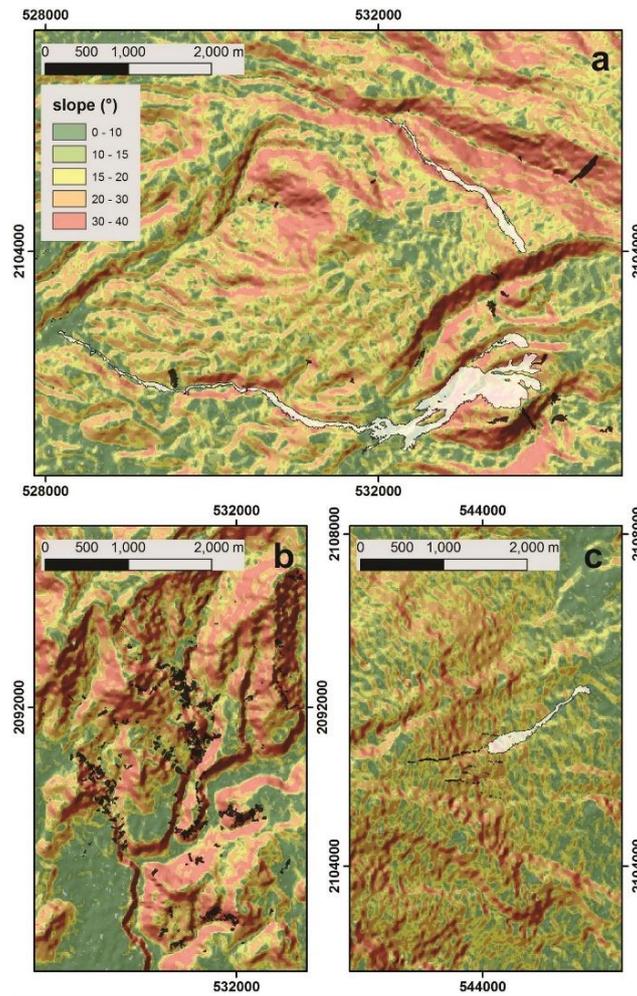
Figure 3: ~~Zoom~~Details of the ~~three~~most afffected areas of the Popocatépetl volcano ~~most affected areas~~ by co-seismic landslides. Black polygons correspond to shallow-landslide scars and deposits, whitish areas ~~dashed line refer~~indicate ~~to the distribution of the~~ debris flows ~~deposits~~. Location of the a, b and c squares are ~~indicated~~reported in ~~f~~Figure ~~3~~2.

We ~~performed~~conducted four field campaigns ~~Field data work were collected~~ from October 2017 to ~~March~~ November 2019

to investigate the morphology and stratigraphy of the source area of main landslides, to map and measure faults and fractures

caused by the earthquake, and to define the extension, thickness and textural characteristics of the larger debris flows (Figure

4). The stratigraphy on the main landslide scars was ~~carefully described~~reconstructed ~~and samples~~ to determine texture and

physical properties of the tephra layers involved in the mass wasting ~~proces~~process. We selected ~~A~~a soil sample ~~in an~~

~~outcrop has been select~~ for radiocarbon analysis to identify the age of the stratigraphic sequence~~,~~ and to define ~~their area~~its

distribution ~~based on previous works (e)~~. The 14C age has been obtained through accelerator mass spectrometry ~~AMS~~dating

(BETA Analytic Laboratory) and calibrated with the IntCal20 calibration curve (Reimer et al., 2020). We mapped and sampled ~~M~~main debris-flow deposits and ~~were mapped and sampled for grainsize analysis. Samples were collected on the landslide scars as well as on the debris flow deposits to perform~~ grainsize analysis were performed~~,~~ by dry-sieving for the sand fraction and by means of a laser particle sizer (Analysette 22) for silt and clay fractions.

215 We analyzed two Sentinel-1 SAR images (Synthetic Aperture Radar, COPERNICUS program) to define the timing between the earthquake and the observed mass wasting processes (Figure 9). The analyzed images were acquired before and after the earthquake (17 and 23 September 2017) in 1A level Ground Range Detected, ascending orbit, Interferometric Wide sensor mode and dual-polarization. A radiometric calibration was applied to extract the most significant amount of backscattering information from the ground linked to the surficial roughness. As a second step, a change detection technique named Log-

220 Ratio was applied to detect pixel values directly related to radar backscattered correlated to superficial processes; this is an algorithm used to detect changes using a mean ratio operator between two images of the same area but taken at different times (Mondini, 2017; Singh, 1989). Finally, ~~W~~we ~~obtained~~analyzed ~~Hydro meteorological~~rainfall data ~~were available from~~ gathered at the Altzomoni raingauge station (ALTZ, Figure 1b)~~,~~ located at approximately 10 km north from the volcano summit.
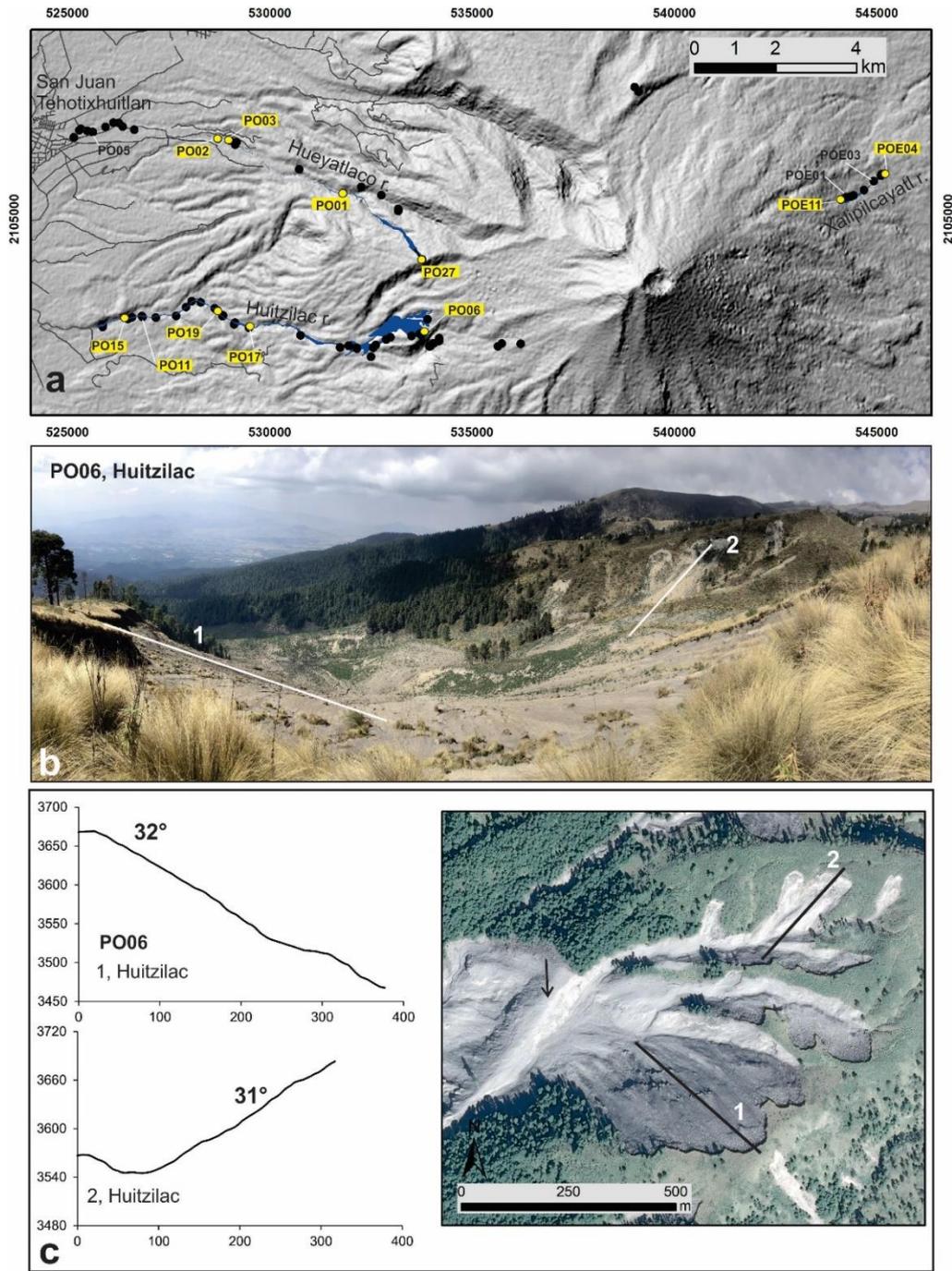
Figure 4: (a) Map of three ravines of the Popocatépetl volcano interested by the debris flows, black dots indicate locations of field surveys (background: 12.5m DEM ©JAXA/METI ALOS PALSAR 2008~~);~~). (b) View in the downstream direction from the top of the sampling point PO~~19~~06, located on the scarp of the Huitzilac landslide ~~n. 1;~~. (c) ~~the~~ Topographic profiles of the larger landslides (1 and 2) ~~n. 1 and n. 2~~that occurred at Huitzilac, which are also reported on the Pléiades 1A image acquired on 13 November 2017; ~~shown in (c) are indicated with white lines. (c) Profiles of the larger landslide scarps.~~the black arrow indicates the topographic barrier overtopped by the debris flow.

4 Results

4.1 Landslide mapping

The earthquake triggered hundreds of shallow landslides (volume > 10³ m³) on the volcano slopes for a total area of 3.8 km² (Figure 2). A total area of 58 km² was interested by sShallow soil slips affecteding the modern soil and part of the unconsolidated volcaniclastic cover. The five largest slope failures are locatedoccurred in the basins of Hueyatlaco and Huitzilac on the West side of the volcanic edifice, and in the basin of Xalipilcayat on the East (Figure 4). The scarps of these landslides were generated at elevations of about 3400-3800 m a.s.l. on the internal faces of ravines or glacial cirques, where slopes are >20° (Figure 4c). In the Hueyatlaco basin, where some of the larger landslides occurred, sSharp rectilinear extensional fractures and small normal faults parallel to the valley slopes were observed in the Hueyatlaco basin after the earthquake (Figure 5a). These faults and fractures opened during the earthquake and land-sliding event, have maximum length of about 1 km, show displacements of up to 40-50 cm and are located on the valley flanks (Figure 5b), suggesting a correlation with local gravitational instability triggered by seismicity. A second cluster of smaller shallow landslides is visible on the southwestern side of the volcanic cone (Figure 2c). These landslides were produced by the collapse of the steep slopes of hummocky hills (dashed circle in Figure 3bFigure 2) that corresponding to the debris avalanche deposit of the last major flak failure occurred at 23.5 ka PB (Espinasa-Perena and Martín-Del Pozzo, 2006; Siebe et al., 2017).
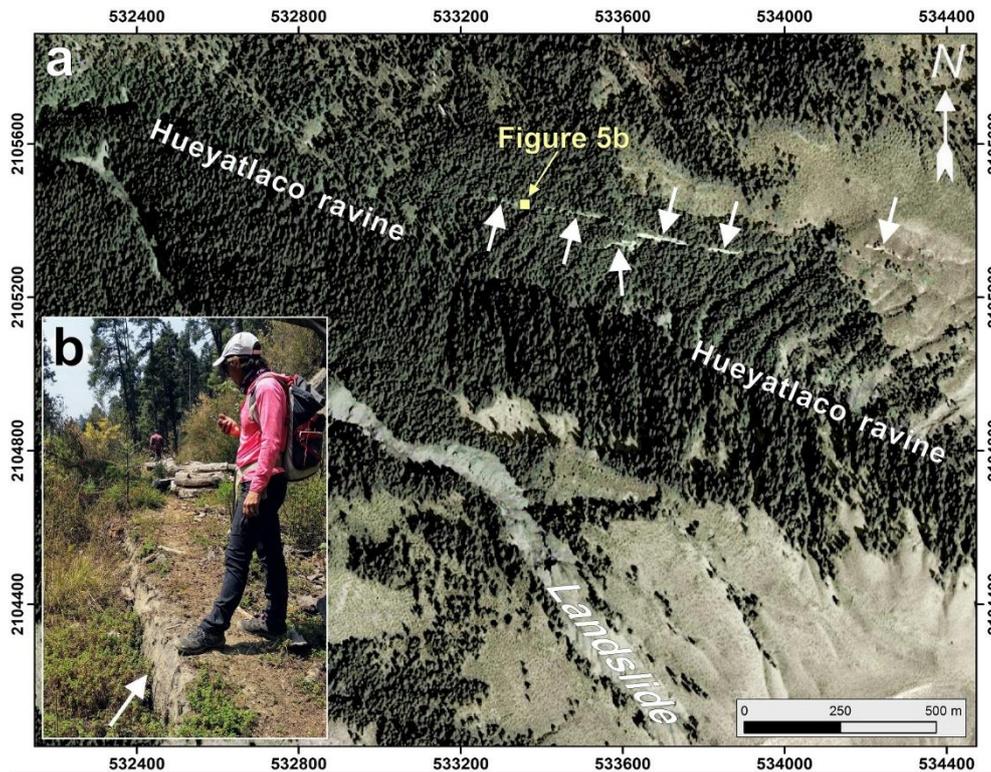
Figure 5: (a) Rectilinear extensional fractures and small normal faults opened parallel to Hueyatlaco ravine (white arrows), background image: Pléiades 1A image acquired on 13 November 2017. (b) Detail of the normal displacement of about 50 cm (white arrow).

The scarps or the larger landslides located on the western slope of the volcano show a ~~very~~ similar stratigraphy, with the intercalation of pumice- and ~~ash~~ ash-fall deposits (Figure 6a-c). Pumice-fall deposits consist of open-framework, clast-supported units~~,~~ composed of ~~with~~ gravel-sand sized fragments of pumice~~,~~ embedded in a matrix of ~~barren of any~~ fine material (from silt ~~or~~ to clay) ~~into the voids (Table 2)~~. Two main layers of pumice-fall deposit~~s~~ were observed at ~~both~~ the Hueyatlaco and Huitzilac ~~main~~ landslide scars (layers B and D, section PO1906; layers C and E, section PO1927, Figure 6e). ~~A third~~Also, another ~~pumice~~ pumice-fall deposit ~~is outcropping~~crops out at the base of the ~~sequence~~pyroclastic succession. The fallout deposits are intercalated with massive o stratified ash layers, with variable thicknesses up to 4 m. They mainly consist of sand (71-93%), silt (16-1%) and less than 1% of clay (see Appendix A~~Table 2~~). A sample from layer C (section PO~~19~~06) was dated by using C14, giving a calibrated age 537~~2~~-64~~33~~39 AD (1500 ± 30 BP conventional radiocarbon age) (Figure 6e). Based on this age, the two younger ~~pumice~~ pumice-fall deposits are here correlated with the Upper and Lower Classic Plinian Eruptions (UCPES and LCPES) of the late Holocene, which main dispersal axis was towards E and NE (Figure 1b) (Siebe et al., 1996). The thicker deposits of these eruptions crop out on the eastern flank of the volcano, as observed at section PO~~19~~11, and correspond to the scar of the Xalipilcayatl landslide (~~section PO1911; Table 2,~~ Figure 6d). Here, a main unit of ~~pumice~~ pumice-fall deposit (C in Figure 6d) features a total thickness of 3.5 m, and consists of a massive, clast-supported unit, dominated by ~~gravel pumice~~coarse fragments~~,~~ barren of any silt and clay fractions ~~(Table 2)~~. This latter unit ~~is intercalated towards the base by~~lies on a 10 cm-thick sandy layer (B~~,~~ in Figure 6d). In all the studied sections, the upper ash unit corresponds to the products accumulated from the frequent vulcanian explosions that characterize the modern eruptive activity of the volcano.

Table 1: Main morphometric data of the landslides that occurred in the headwaters of Hueyatlaco, Huitzilac and Xalipilcayatl ravines. The area of the main scars was inferred ~~from field surveys and~~ from the inspection of post-event optical images (see Figure ~~6~~8). The depth of the scars was measured in the field. The volume of the landslides was calculated assuming a constant depth (with an uncertainty of ±0.5 m) over the area of detachment.

	Max elevation (m)	Area (m²)	Depth (m)	Slope (°)	Volume × 10³ (m³)
Hueyatlaco	3 860	60 000	4	29	240 ±30
Huitzilac	3 700	310 000	3	31-32	930 ±155
Xalipilcayatl	3 500	60 000	3	25	180 ±30
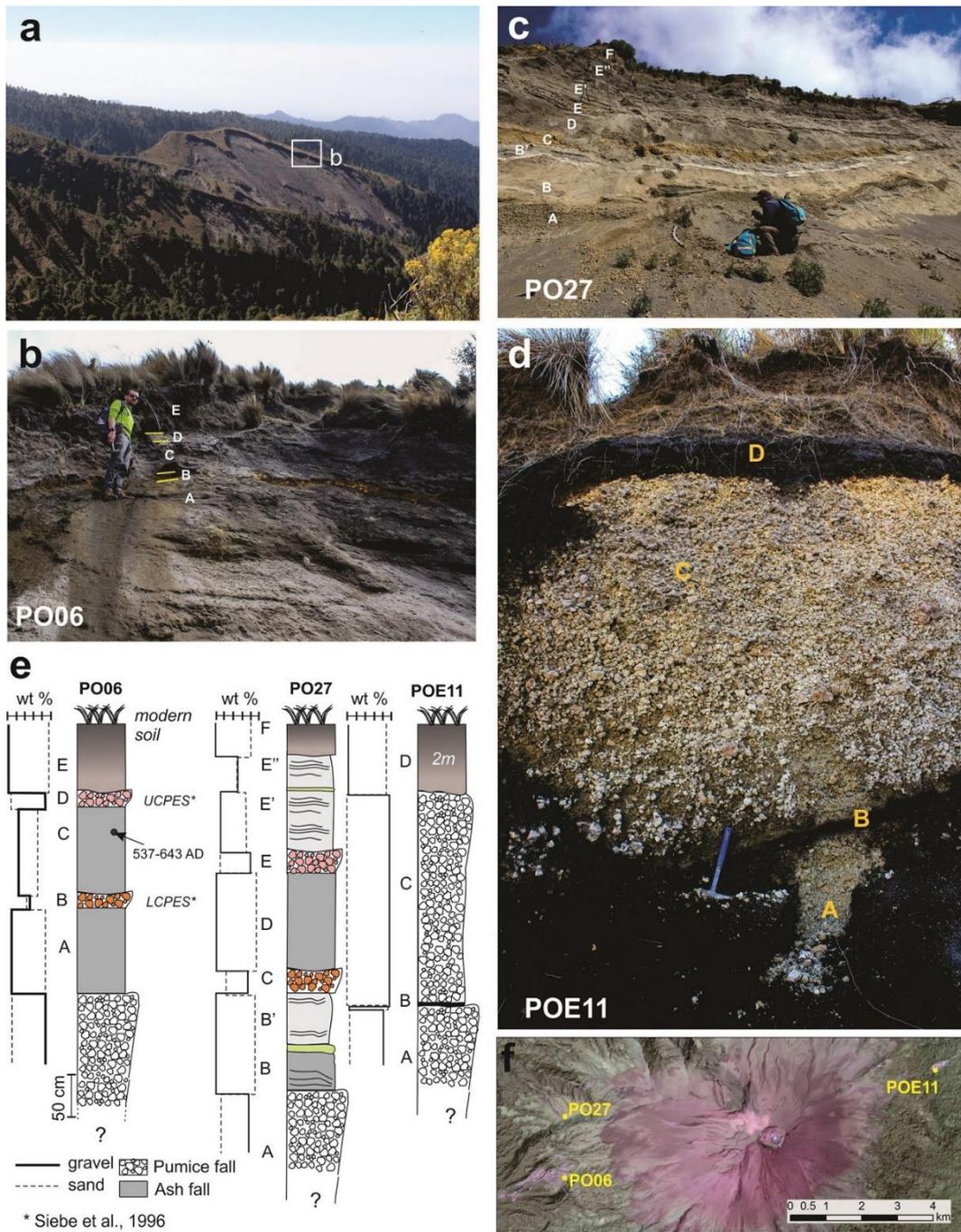
Figure 6: View of the three main landslides scarps: (a, b) Huitzilac, (c) Hueyatlaco, (d) Xalipilcayatl. In (e) the stratigraphic sections of the three scarps are reported, see text for more details. (f) Geographic location of sampling points, background image: Pléiades 1A image acquired on 13 November 2017.

4.2 Characterization of debris flows and associated deposits

The five largest landslides described in Section 4.1 (one at Hueyatlaco and Xalipilcayatl, respectively, and three at Huitzilac) mobilized a total volume of about 1.35 × 10⁶ m³ of ash- and ~~pumice~~ pumice-fall deposits (Table 1). ~~Main~~ Landslide scarps ~~of the largest slope failures are located at elevations ranging from 3400 to 3800 m a.s.l. and~~ measure ~~400~~ 640 m of length and 4 m of depth at Hueyatlaco, ~~700~~ 740 m of length and 3 m of depth at Huitzilac, and ~~200~~ 400 m of length and 3 m of depth at Xalipilcayatl (Figure 7). We calculated the ~~The~~ volume of the landslides ~~was calculated~~ by assuming a constant depth (with an uncertainty of ±0.5 m) over the area of detachment. We measured ~~The~~ the depth of the main scars ~~was measured~~ in the field while the area of the main scars was inferred from field surveys and from the inspection of post-event optical images (Figure 7).
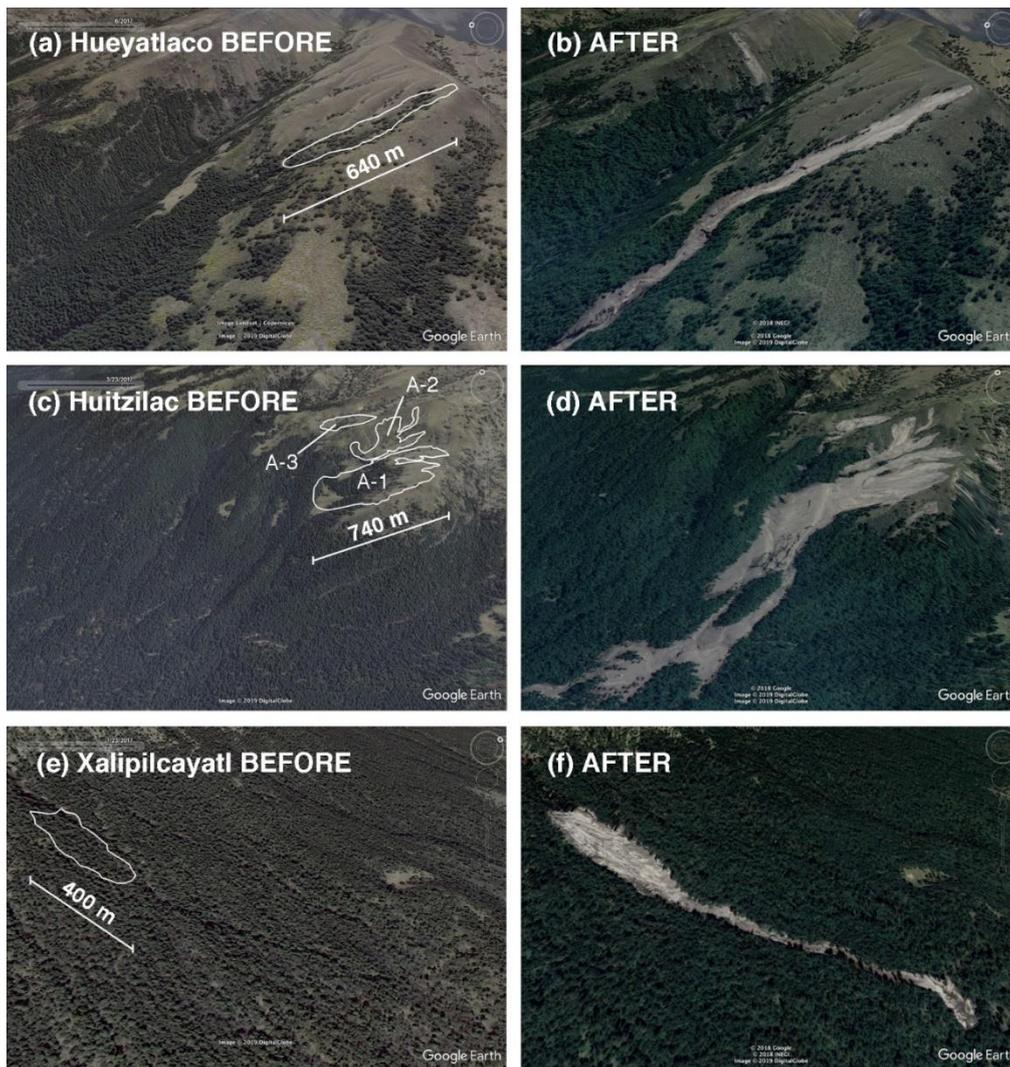
Figure 7: Comparison of 3D views on the detachment areas in the headwaters of Hueyatlaco (a,b), Huitzilac (c,d) and Xalipilcayatl (e,f) ravines before and after the larger ~~Major~~ landslides ~~that occurred in the headwaters of Hueyatlaco, Huitzilac and Xalipilcayatl ravines.~~ ~~Comparison of 3D views on the detachment areas before and after the landslides.~~ Images from Google Earth (©Google 2018, ©INEGI 2018 and ©DigitalGlobe 2019).

295 The landslides transformed into three long-runout debris flows (Figure 8). At Huitzilac ravine, the main landslide body (landslide A-1) impacted on the opposite side of the valley, partly overtopping it (Figure 4c and 8a). Two other soil slips (landslide A-2 and A-3, Figure 7) contributed forming the subsequent debris flow, which extended up to 7.7 km from the source before diluting into a streamflow. The total observed thickness of the deposit measures up to 3 m, but mud traces on standing trees and on lateral terraces measure up to 10 m on proximal reaches (PO~18~17, Figure 8b) and up to 1.5 m in distal

300 reaches with horizontal surfaces at benches (PO11, Figure 8f). In distal reaches, where the channel was shallow, the flow inundated large plains (PO~18~15 and PO~18~19). The deposit is massive, dark-gray in color, which mainly consists of sand (77-86%) with a relevant gravel proportion (15%) due to pumice fragment enrichment in proximal reaches (Figure 8i~Table 2~). Clay content is less than 1%. The lower unit consists of coarse-to-medium ash~, mainly sandy,~ with evidence of dewatering (Figure 8g). At Hueyatlaco, the debris-flow runout extended up to 6.4 km (Figure 4). The deposits appears as a main unit,

305 dark-gray in color, massive and homogeneous whose sand fraction consists of 70% in proximal reaches (PO~17~01) to 87% in distal reaches (PO~17~05), with up to 15% of silt and less than 1% of clay (Figure 8i, ~Table 2~see also Appendix A). Overbank deposits show sharp edges up to 10-cm thick (PO~17~02, Figure 8e). The total observed thickness is up to 50 cm (Figure 8d, erosion was only incipient at the time of the observation) but watermarks up to 5 m were observed in proximal reaches (PO1701, Figure 8c). Finally, the deposit in the Xalipilcayatl ravine extended up to 1.5 km (Figure 7f) and is clearly

310 composed of two main units. The lower unit is massive, dark-grey in color and mostly consists of sand fraction (88%, POE03-lower, Figure 8i ~Table 2~), up to 1.2 m in thickness, while the upper one is massive, pumice-enriched and represents up to 40% of the total unit (POE04, Figure 8h and 8i).

~~**Table 2:** Grain size distributions of selected samples collected in the landslide scarps and deposits. Refer to Figure 4 for sample locations.~~

~~Landslide scars~~				
~~PO1906~~	~~Gravel (wt %)~~	~~Sand (wt %)~~	~~Silt (wt %)~~	~~Clay (wt %)~~
~~E~~	~~3.49~~	~~93.14~~	~~3.29~~	~~0.09~~
~~D~~	~~87.01~~	~~11.94~~	~~1.00~~	~~0.05~~
~~C~~	~~26.47~~	~~71.90~~	~~1.61~~	~~0.03~~
~~B~~	~~54.36~~	~~45.12~~	~~0.51~~	~~0.01~~
~~A~~	~~13.92~~	~~81.00~~	~~4.95~~	~~0.13~~
~~PO1927~~	~~-~~	~~-~~	~~-~~	~~-~~
~~F~~	~~0.36~~	~~82.18~~	~~16.78~~	~~0.68~~
~~E″~~	~~45.75~~	~~53.30~~	~~0.91~~	~~0.04~~
~~E′~~	~~10.25~~	~~76.50~~	~~12.73~~	~~0.52~~
~~E~~	~~80.98~~	~~16.39~~	~~2.45~~	~~0.17~~
~~D~~	~~1.49~~	~~87.28~~	~~11.12~~	~~0.10~~

C	71.66	27.88	0.45	0.01
B'	0.10	83.89	15.31	0.70
B	0.50	83.77	15.39	0.33
A	80.06	12.40	6.98	0.57
PO1911	-	-	-	-
D	0.53	88.55	10.66	0.26
C	94.81	5.19	0.00	0.00
B	4.12	91.84	3.87	0.16
A	89.16	10.37	0.43	0.04
Debris-flow deposits				
Hueyatlaco ravine	-	-	-	
PO1701	17.98	69.20	12.22	0.61
PO02A	19.49	79.05	1.37	0.09
PO02B	5.65	86.42	7.78	0.15
PO02C	4.76	87.52	7.56	0.16
PO05A	6.46	77.81	15.19	0.54
PO05B	2.91	80.49	15.95	0.66
Huitzilac ravine				
PO11	4.25	86.21	9.19	0.34
PO15	0.09	83.54	15.82	0.52
PO17	15.35	77.02	7.41	0.20
PO19	8.49	77.96	13.15	0.38
Xalipilcayatl ravine				
POE04	58.75	36.69	4.25	0.30
POE01	30.77	60.26	8.59	0.36
POE03 upper	62.93	34.45	2.41	0.20
POE03 lower	0.69	88.32	10.63	0.34

We estimate a total entrainment of about 205 000 m³ along both hillslopes and channel network assuming 0.5 m of erosion over the area located downstream from the main scars (Table 32). Large wood (LW) elements entrained by the initial landslides and the subsequent debris flows contributed to the final bulk deposits of about 1.632×10^6 m³. The volume of LWs was calculated considering a mean tree height of 25 m (measured in the field, with an uncertainty of ±5 m), a mean trunk diameter of 0.4 m (observed in the field, with an uncertainty of ±0.1 m) and a mean distance of two trees of 10 m (estimated by using the post-event optical images, see Figure 7). The amount of LW recruited in the Huitzilac basin results in 60 000 m³ (±3 000 m³), far more than the sum of Hueyatlaco (10 000 ±500 m³) and Xalipilcayatl (7 000 ±350 m³) basins. The recruited LW stemmed from the combination of hillslope and channel processes originated from the earthquake-induced landslides. In general, these landslides were the dominant recruitment processes in headwaters. In contrast, LW recruitment from lateral bank erosion became significant in the intermediate reaches of the channels. The slope area collapsed into the

Xalipilcayatl basin contained most of the LWs afterwards transported by the flow (86%). In the Huitzilac basin, the LW recruitment mainly occurred on the slopes located right below the collapses (62%), while in the Hueyatlaco basin on the channel banks (75%). Most of the transported LWs remained trapped by natural obstacles in the main channel (i.e. standing vegetation) and clogged in the flat reaches of the channel (Figure 8d). In the Xalipilcayatl ravine, most of LWs were transported for the whole runout distance into the main landslide deposit (Figure 9i).
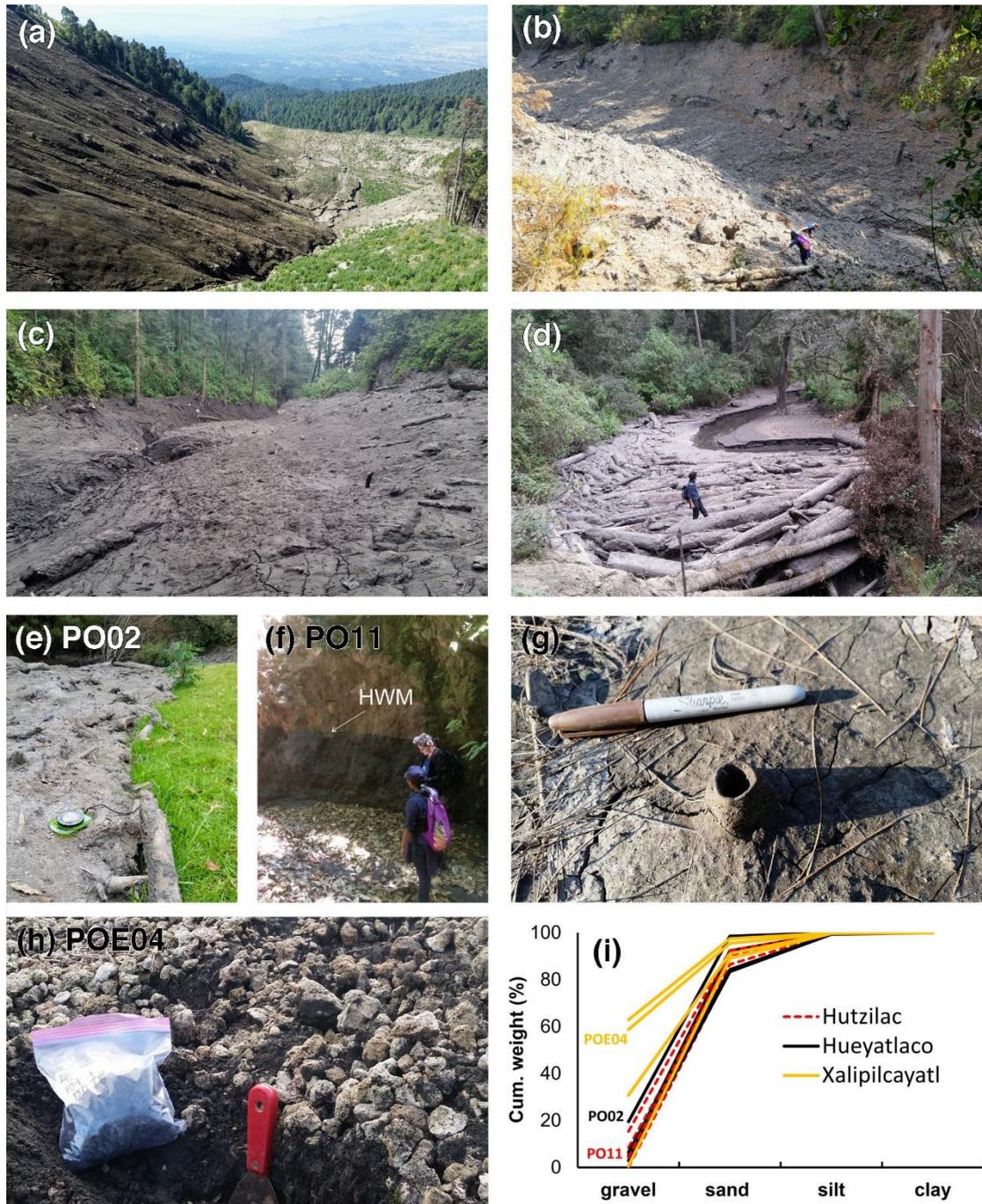
Figure 8: Debris-flow deposits in the upper (a-c), intermediate (d-f) and lower reaches (g-h) of Huitzilac, Hueyatlaco and Xalipilcayatl basins: (a) scarp of landslide A-1 at Huitzilac (view from point PO~~19~~06), (b) main channel of Huitzilac ravine (PO~~18~~17), (c) main channel of Hueyatlaco ravine (PO1701), (d) large wood deposits at Hueyatlaco (PO03), (e) overbank deposits at Hueyatlaco (PO~~17~~02), (f) mud trace on lateral terraces at Huitzilac, HWM = Height of Water Mark (PO11), (g) evidence of dewatering at Huitzilac (PO~~18~~19), (h) detail of the lower deposit at Xalipilcayatl (POE04), (i) grainsize distribution of selected samples. ~~main channel right upstream the deposition area at Xalipilcayatl.~~

Table ~~3~~2: Main morphometric data of the debris flows that were observed in the Hueyatlaco, Huitzilac and Xalipilcayatl basins. The entrained volume was calculated assuming 0.5 m of erosion over the area located downstream from the main scars where the vegetation was destroyed. The volume of large wood (LW) fragments was calculated considering a mean tree height of 25 m (with an uncertainty of ±5 m), a mean trunk diameter of 0.4 m (with an uncertainty of ±0.1 m) and a mean distance of two trees of 10 m.

	Runout (km)	Drop height (m)	Entrainment $\times 10^3$ (m³)	LW volume $\times 10^3$ (m³)
Hueyatlaco	6.4	1 160	50	10 ± 0.5
Huitzilac	7.7	1 200	120	60 ± 3
Xalipilcayatl	1.5	350	35	7 ± 0.35

4.3 Timing of the events

Results of Sentinel-1 SAR image processing clearly indicate that both landslides and debris flows had already occurred between 17 and 23 September 2017. A binary image was produced where pixels values are linked to spatial change that occurred in this spam of time (Figure 9a). Their distribution corresponds with the deposits of the larger debris flows that occurred in Huitzilac and Hueyatlaco basins, as it is easily observable in a later optical Sentinel-2 image (COPERNICUS program) acquired on 18 October 2017 (Figure 9b).
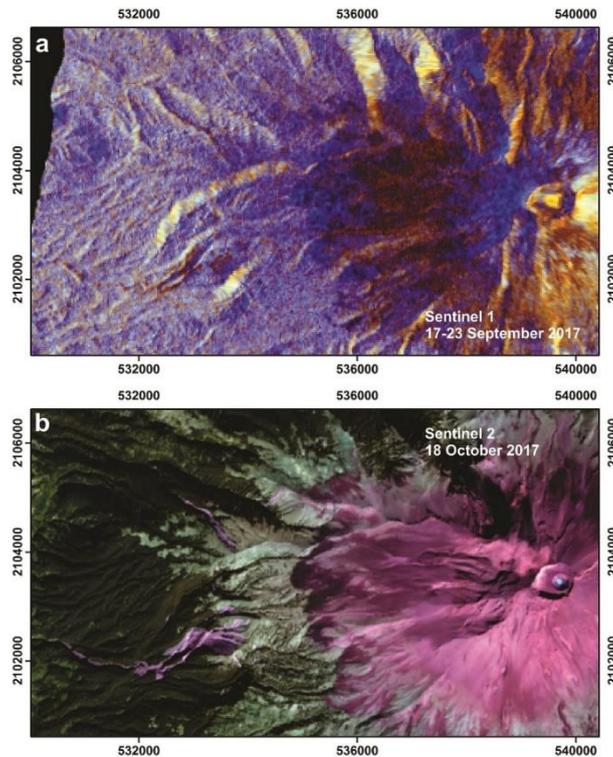
Figure 9: (a) RGB (R, post-earthquake; G, pre-earthquake; B, ratio between post- and pre-event) representation of the 17 and 23 September Sentinel-1 (©Copernicus data) change in amplitude analysis; (b) RGB composition of post-event Sentinel-2 image (©Copernicus data).

A total of 200 mm of accumulated rainfall were recorded during the 30 days preceding the earthquake, with the accumulation of 19.7 mm two days before the earthquake (Figure 10). Thus, we expect that the slope material was wet at the

355 time of the earthquake. Based on the remote sensing analysis and considering that between 19 and 23 September only a few mm of rainfall accumulated (Figure 10), it is thus highly probable that both slope failures and debris-flow emplacement were co-seismic. Witnesses from the town of Atlautla, which is located at the outlet of Huitzilac ravine (Figure 1b), also confirmed this information. During the following weeks, rainfalls remobilized fine material from the landslide deposits reaching the town of San Juan Tehuixtitlán (Figure 4a). On 4 October 2017, the population of San Juan Tehuixtitlán noticed

360 the transformation of the shallow water-flow of Hueyatlaco ravine into a hyperconcentrated flowhigh concentrated, slow-moving debris flow. It is-was the first time that this local community located on the western volcano slope observed such a phenomenon. Rainfall measurement at Altzomoni raingauge station (ALTZ, Figure 1b) shows an accumulation of 35.7 mm of rainfall over 12 hours since 10 hrs (UTC time) of 4 October, with a peak between 20 and 21 hrs (Figure 10). The rainfall event of 4 October only remobilized fine material from the landslide deposits reaching the town of San Juan Tehuixtitlán; the

365 debris flows along the Huitzilac and Xalipilcayatl were never reported since they never extended out to any populated area in 2017. During the 2018 and 2019 rainy seasons, the fine sediment remobilized from the debris-debris-flow deposit in Huitzilac ravine reached the bridge of the road connecting San Juan Tehuixtitlán Amecameca-to Atlautla (Figure 1b).
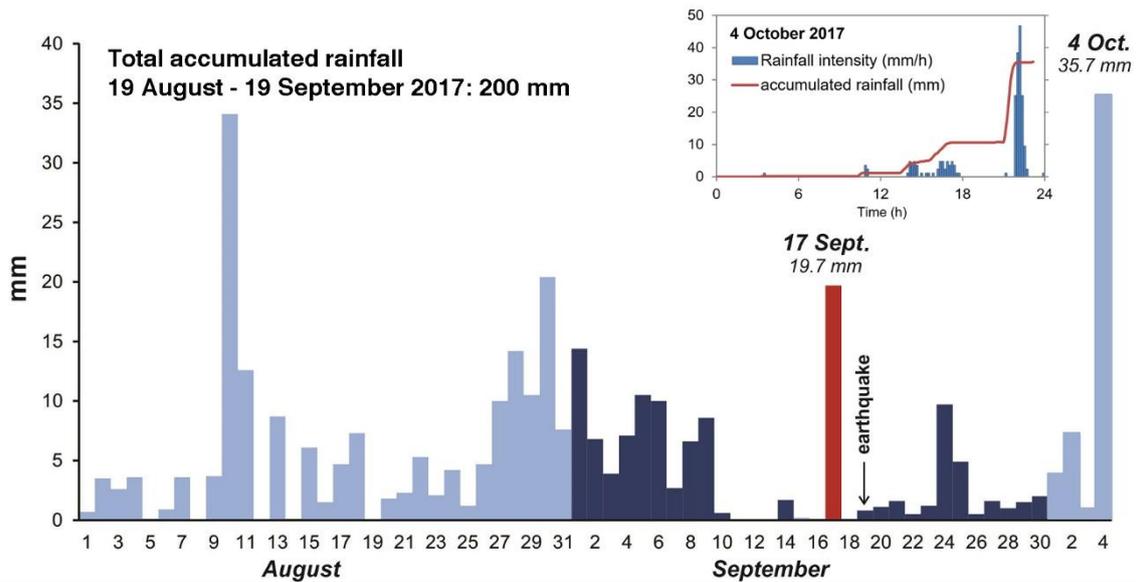
Figure 10: Rainfall measurements at rain gauge ALTZ from 1 August to 4 October 2017. A total accumulated rainfall of 200 mm was
370 recorded during the 30 days preceding the earthquake, 19.7 mm of which on 17 September 2017 (red bar). On 4 October 2017, the population of San Juan Tehuixtitlán noticed the passage of a sediment-laden flow in Hueyatlaco ravine.

5 Discussion

5.1 Predisposing factors to slope instabilities

Popocatépetl area is tectonically characterized by a Quaternary roughly NE-SW/ENE–WSW trending maximum horizontal
stress regime, responsible for arc-parallel E-W-striking transtensive faults and NE-SW/ENE–WSW arc-oblique normal faults (Arámbula-Mendoza et al., 2010; García-Palomo et al., 2018; Norini et al., 2006, 2019). This stress regime generated ENE–WSW extensional fracturing and faulting of the volcanic edifice (Figure 11), controlling the orientation and propagation by magmatic overpressure of dikes within the volcanic cone and recent eruptive fissures on its flanks (Arámbula-Mendoza et al., 2010; De Cserna et al., 1988).

~~On 19 September 2017, Popocatépetl volcano underwent co-seismic slope failures.~~ The size of the~~se~~ slope failures triggered by the 2017 M$_W$ 7.1 Puebla-Morelos earthquake ~~greatly changes with the location with respect to the cone's summit,~~is highly variable although (i) the epicenter of the earthquake is far from the volcano, with seismic shaking expected to be of similar intensity all over the symmetric volcanic cone, and (ii) soil and recent pyroclastic cover is quite homogeneous on the edifice flanks. Small shallow landslides occurred all over the volcano flanks, while the few larger landslides described in our work are limited to the eastern and western sides of the volcanic cone (Figure 2). Thus, seismic shaking originated by the ~~far~~ earthquake triggered large (volume $> 10^5$ m^3) landslides only in specific sectors of the volcano flanks.
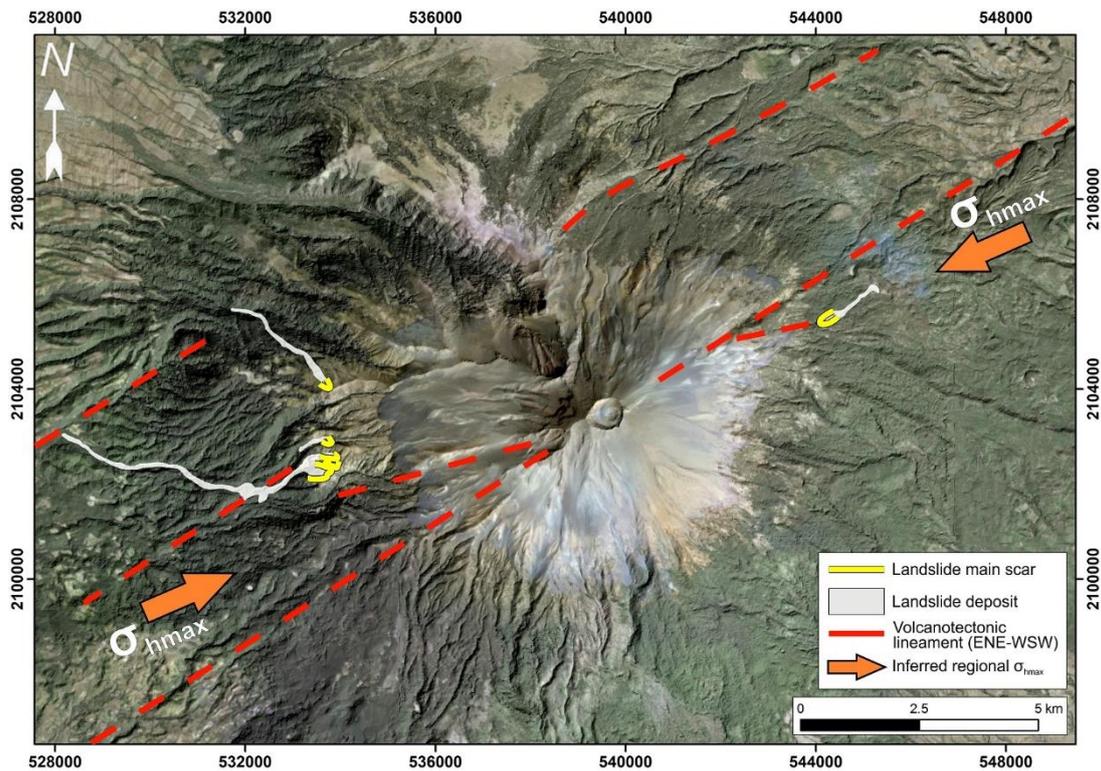
Figure 11: Simplified tectonic setting of the Popocatepetl area and location of the main earthquake-induced landslides that occurred on 19 September 2017. Background image: ©DigitalGlobe/ESRI 2019.

The location of the larger slope failures defines a sharp ENE-WSW unstable sector crossing the volcano summit and parallel to many deep rectilinear valleys carved in the volcanic cone (Figure 11). In this ENE-WSW elongated sector of the volcano, some faults and extensional fractures have been generated by the 2017 earthquake in the same basins where the larger landslides occurred (Figure 5). This configuration may suggests strongly localized site effects and/or a structural control on the location of the slope instability. Indeed, the unstable sector is roughly parallel to the ENE–WSW maximum horizontal stress, where local volcanotectonic structural features are recognized on the volcano (Arámbula-Mendoza et al., 2010; De Cserna et al., 1988). The remobilization of larger quantities of material in this sector with respect to other areas of the volcano flanks may be correlated to the presence of ENE-WSW–striking faults and fractures that progressively weakened the volcanic edifice. Some of these volcanotectonic structures may also have undergone transient reactivation by seismic shaking, increasing local slope deformation by opening of fractures that promoted the largest slope failures triggered by the earthquake.

5.2 Initiation of co-seismic landslides

Slopes collapse when the shear stress across a potential failure plane exceeds the substrate strength. Earthquakes reduce the slope stability and can cause landslides through the perturbation of the normal and shear stresses in the slope. In case of soft, saturated soils, the coalescence of cracks during earthquakes may results in liquefaction due to the increase of substrate permeability. At Popocatépetl volcano, a combination of these two mechanisms produced the soil slips observed in the headwaters of Hueyatlaco, Huitzilac, and Xalipilcayatl basins. Shapiro et al. (2000) already noticed that a large earthquake occurring in the vicinity of the volcano may result in flank instability because of the seismic waves traversing the poorly consolidated material composing the volcanic edifice. The ground motion during the 2017 earthquake was anomalously large in the frequency range 0.4–1 Hz, as intraslab earthquakes involve higher stress drop than their interplate counterparts (Singh et al., 2018). Consequently, the ground motion is relatively enriched at high frequencies as compared with that during interplate earthquakes, which is dominated by lower frequency waves (f< 0:5Hz), and this can contribute explaining the high value of PGA measured on the volcano slope.

Unexpected large peak accelerations have been recorded along crests of mountain ridges during several earthquakes (Davis and West, 1973; Meunier et al., 2008). Topographic amplification of ground vibrations is primarily due to the reflection/diffraction of seismic waves, which are progressively focused upwards (Bouchon et al., 1996; Davis and West, 1973). and the The constructive interference of their reflections and the associated diffractions of seismic waves increases towards the ridge crest also due to local geologic factors, giving rise to enhanced ground accelerations on topographic highs (Del Gaudio and Wasowski, 2007; Meunier et al., 2008; Von Specht et al., 2019). Geli et al. (1988) show that the topographic complexity (presence of neighboring ridges) may be responsible for large crest/base amplifications resulting in complex amplification-deamplification patterns and significant differential motions along the slopes. The amplification at the

crest of a mountain can be as large or larger than the amplification normally caused by the presence of near-surface unconsolidated layers (Davis and West, 1973). It is well-known that shallower earthquakes may cause large landslides (e.g., Marc et al., 2019), but the Puebla-Morelos earthquake was moderately deep (i.e., 57 km). The PGA produced by the 2017

425 earthquake at station PPIG (~~158.16~~106.83 cm/s^2) was about ~~three~~ two times higher than the PGA observed at CU (57.1 cm/s^2). Indeed, the distance epicenter-PPIG (68 km) is about half than the distance epicenter–CU (111 km) and this partially explains the difference in PGA observed at the two stations. However, during the earthquake the headwaters of Hueyatlaco, Huitzilac, and Xalipilcayatl ravines could have experienced even higher values of PGA due to the effect of topographic amplification of seismic waves. The PGA map produced by the USGS Seismic Hazard Program shows values between 0.28g

430 in the southern sector of the cone and up to 0.18g closer to the vent (Figure 2c). The spatial interpolation of PGA clearly shows the interaction between the energy distribution and the topography, which played an important role in the location of landslides. The cluster of smaller landslides located on the southwestern side of the volcanic cone, closer to the epicenter, is likely due to the combination of large ground motion and high slopes that consist of debris avalanche hummocks (Figure 3b). The complex topography of Popocatépetl volcano, characterized by neighboring ridges and valleys, probably produced local

435 amplification values that makes it difficult to explain why larger soil slips did not occur in other similar locations in terms of elevation, slope and stratigraphy. However, the deposits located along the ENE-WSW unstable sector of the volcano (see ~~previous paragraph~~section 5.1), at an elevation ranging from 3400 to 3800 m and characterized by a slope > 20°, appear as the most likely to suffer collapse in case of an earthquake. This sector of Popocatépetl volcano consists of a mantle of loose volcaniclastic material with the intercalation of silty-sandy ash layers and gravel-sand pumice fall deposits (up to 5-m thick,

440 see Figure 6), covered by a modern soil with thick alpine grassland. At higher altitude, the steeper slopes are unvegetated, and consist of unconsolidated pyroclastic granular material where superficial granular flows can be easily observed. The largest landslides occurred in the limit of the vegetation line, where pine tree became scattered but grassland is still abundant (Figure 7a, c). The intercalation of layer with different grainsize and the soil coverage are probably promoting water accumulation. Indeed, one mechanism that possibly can explain the collapse of this material is the liquefaction through the

445 disruption of internal, suspended aquifers. A similar observation was recently made at Nevado del Huila Volcano, Colombia, during 2007 when lahars originated after large fractures formed across the summit area of the volcano in consequence of a strong hydromagmatic explosion that drained small, perched aquifers (Johnson et al., 2018). On the unvegetated portion of the cone, mass remobilization processes such as raveling and superficial granular flows likely occurred but without leaving any scarp, because of the lack of a compacted soil.

450 **5.3 Transformation into long runout debris flows and implications for hazard assessment**

Once generated, the earthquake-induced soil slips transformed into debris flows. The two major debris flows that occurred in Hueyatlaco and Huitzilac basins covered a runout distance of 6.4 and 7.7 km, respectively. In Figure 12, we show the conceptual model of this transformation at Popocatépetl volcano: the propagation of an earthquake-induced crack in the slope (1) produces a shallow landslide composed of a mix of ash and pumice (2). The collapsed material disaggregates and

455 impacts on the opposite side of the valley and rapidly the landslide evolves into debris flows, due to the high-water content of the collapsed unconsolidated material (3). The subsequent debris flow is highly viscous due to the high sand and silt fraction of the mixture (Figure 8i) and contains abundant LWs entrained along the channel network, especially along the Huitzilac and Xalipilcayatl channels which had entire mature trees incorporated, thus leaving abundant log-strewn debris. Even if no direct observations are available to assume if the collapsed slopes were partially or completely saturated, it is

460 clear that debris flows contained a large amount of water as observed from dewatering features of the deposits and high-water marks along the channels (Figure 8g). Since August 21, 138 mm of rainfall accumulated continuously for two weeks, and 19.7 mm just two days before the earthquake (Figure 10). This large amount of rainfall was then stored in the open-framework pumice fall deposits intercalated by m-thick sandy layers, and in the root fabric of the trees in the dense forest cover.
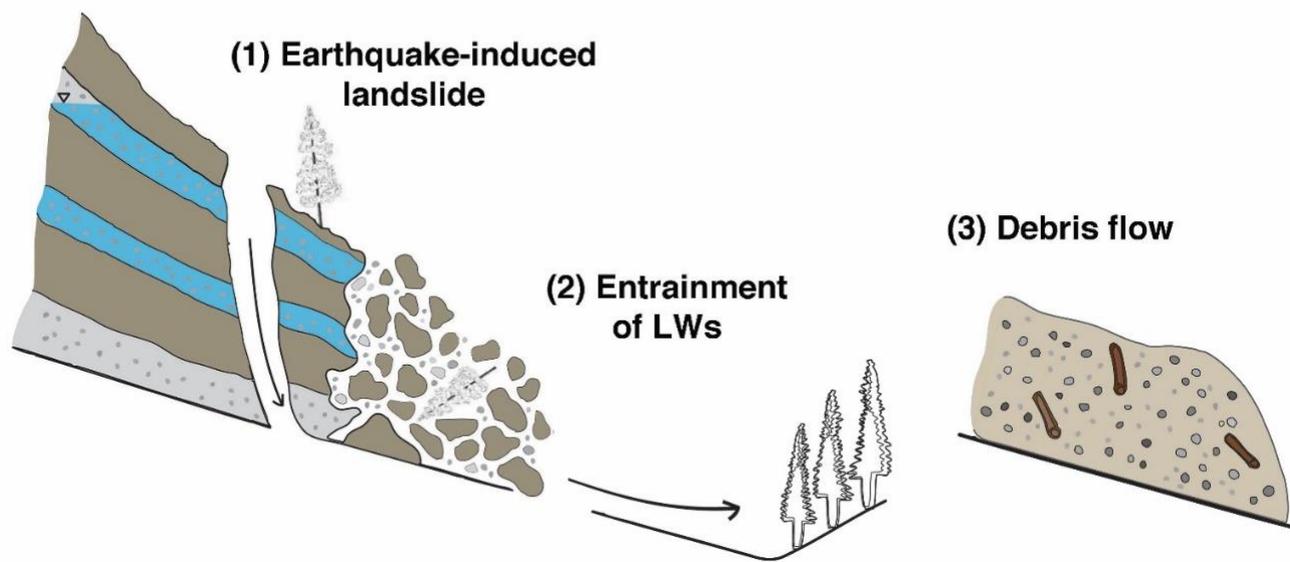
465

Figure 12: Conceptual model of transformation of earthquake-induced soil slips into debris flows at Popocatépetl volcano: (1) the earthquake produces the collapse of the saturated slope composed of a mix of ash and pumice; (2) the landslide impacts on the opposite side of the valley entraining large amount of Large Woods (LWs) and (3) evolves into a debris flow due to the high-water content of the material. The simplified stratigraphy in (1) reflects the one observed at the scar of Huitzilac landslide (see Figure 6c).

470

Volcanoes store or drain water in and through aquifers that can grow and empty, as impermeable barriers develop or as they are breached by deformation, respectively (Delcamp et al., 2016). Even if not completely saturated, ground vibrations induced positive pore pressure and triggered liquefaction and slopes failure (Kameda et al., 2019; Wang et al., 2019). It is important to note that on August 10 a rainfall of 35 mm, similar to the October 4 event that triggered the sediment-laden

475 flow observed at San Juan Tehuixtitlán village, did not induce any channel response, indicating the stability of the slopes of this sector of the volcano prior to the earthquake. In fact, except for the 2010 lahar that occurred in the Nexplayantla ravine

after 100 mm of accumulated rainfall (Zaragoza-Campillo et al., 2020), lahars are related to major eruptions, reason for which the actual hazard map of the Popocatépetl volcano includes only rainfall-triggered lahar during or after eruptions (Martin Del Pozzo et al., 2017). Detailed field investigations of the role of aquifers on volcanic landslides are very scarce to

480   the date (Delcamp et al., 2016). Knowledge of the distribution of perched aquifers and water content of volcanic deposits can provide precious insights on a complex mass wasting chain like the one that experienced by Popocatépetl volcano in 2017.

Finally, it is worth mentioning that during our last field campaign of November 2019 we observed that the source areas of the larger debris flow that occurred at Hutzilac ravine were becoming stable thanks to the combined effect of the removal of fine material and of the growth of new vegetation. On the contrary, the large amount of material deposited along the channel

485   remains available for remobilization for many years, resulting in a remarkable increase of sediment yield as observed in other locations (e.g., Fan et al., 2021). Indeed, during 2018 and 2019 rainy seasons, the fine sediment remobilized from the debris-flow deposits in Huitzilac ravine reached the road connecting San Juan Tehuixtitlán to Atlautla.

6 Conclusions

The catastrophic event of ~~17~~ 19 September 2017 at Popocatépetl volcano ~~provide a significant~~ is an ~~example~~ exemplary case

490   of interrelated multiple hazards in volcanic environment: earthquakes, landslides, and sediment-laden ~~floods~~flows. Landslides represent one of the most dangerous phenomena that may occur on active volcanoes, even in periods of dormancy. During the M_W 7.1 Puebla-Morelos intraslab earthquake, hundreds of shallow landslides were triggered on the volcano flanks. The combination of strong ground motion due to local amplification ~~earthquakeand~~ with the presence of water-saturated, tephra-rich superficial deposits ~~on volcano slopes can~~ result~~ed~~ in large ~~mass movements~~slope failures and

495   subsequent liquefaction of the collapsed material~~floods that can dramatically increase the sediment load along the drainage network~~. ~~During the September 2017 event,~~ Aa total volume of about 10^6 cubic meter~~s~~ of volcaniclastic deposits ~~collapsed and~~ transformed in~~to~~ two large debris flows on the western slope of the volcano and one on its eastern side. While the source areas rapidly stabilize, the fine material deposited in the channels remains exposed to possible remobilization for many years. ~~This is the first time that such large wood strewn debris flows were directly observed at this volcano.~~ These

500   observations imply the need to revise the hazards assessment for Popocatépetl volcano, where multi-hazard risk scenarios should be taken into account. ~~Seeing such deposits in the geologic record could also cause confusion with identifying them with primary lahars.~~ The here described mass-wasting cascade ~~observed and here described~~ may occur in other areas, especially continental volcanic arcs and mountain chains in seismic regions worldwide.

Acknowledgements. This research is supported by the CONACYT-PN 360 project and the EARFLOW project (2018-2020),

505   funded by the MAECI - Ministero degli Affari Esteri e della Cooperazione Internazionale and the AMEXCID - Agencia Mexicana de Cooperación Internacional para el Desarrollo. Seismic data were provided by the Servicio Sismológico Nacional (SSN - UNAM, México). Rainfall data were kindly provided by Adolfo Magalli. This paper is supported by the Open Access Publishing Fund of the Free University of Bozen-Bolzano. We thank Berlaine Ortega-Flores, Lizeth Cortez and

Lizeth Caballero-García (UNAM) for their support in the field and in the laboratory. We are thankful for constructive feedback from Thomas Pierson on an earlier version of the manuscript. We thank Matteo Roverato and ~~two~~ three anonymous reviewers and the editor X. Fan for their constructive comments and revisions.

Data availability. Samples collected on landslide scars and deposits are stored at CGEO-UNAM. Original data presented in Table 1 and 2 (polygons of the main landslides and LWs) and grain size distribution of the samples are available as supplementary material. The map of the PGA distribution of the M_W 7.1 Puebla-Morelos earthquake (USGS Earthquake Hazard Program) is available at https://earthquake.usgs.gov/earthquakes/eventpage/us2000ar20/shakemap/pga. Sentinel-1 and Sentinel-2 images (©Copernicus data) acquired on 17 and 23 September 2017 are available at https://scihub.copernicus.eu/. Rainfall data at Altzomoni raingauge station (ALTZ, RUOA-UNAM) are available at https://www.ruoa.unam.mx/index.php?page=estaciones. The 50-cm resolution Pléiades (AIRBUS) optical image acquired on 13 November 2017 was bought by the authors.

Author contributions. VC and LC conceived the idea and planned the field activities. VC, LC, GN, DF and EP participated to the field work. VC, LC and GN wrote the manuscript. VM analyzed seismic data of the PPIG station (SSN-UNAM). ND processed Sentinel-1 and Sentinel-2 images. EP, LC and VC analyzed the post-event Pléiades image and drew the landslide map. All the authors discussed the results and commented on the manuscript.

Competing interests. The authors declare that they have no conflict of interest.

Appendix A

Grain size distributions of samples collected in the landslide scarps and deposits. Refer to Figure 4 for sample locations.

Landslide scars				
PO1906	Gravel (wt %)	Sand (wt %)	Silt (wt %)	Clay (wt %)
E	3.49	93.14	3.29	0.09
D	87.01	11.94	1.00	0.05
C	26.47	71.90	1.61	0.03
B	54.36	45.12	0.51	0.01
A	13.92	81.00	4.95	0.13
PO1927	-	-	-	-
F	0.36	82.18	16.78	0.68
E''	45.75	53.30	0.91	0.04
E'	10.25	76.50	12.73	0.52
E	80.98	16.39	2.45	0.17
D	1.49	87.28	11.12	0.10
C	71.66	27.88	0.45	0.01
B'	0.10	83.89	15.31	0.70
B	0.50	83.77	15.39	0.33
A	80.06	12.40	6.98	0.57
PO1911	-	-	-	-
D	0.53	88.55	10.66	0.26
C	94.81	5.19	0.00	0.00

B	4.12	91.84	3.87	0.16
A	89.16	10.37	0.43	0.04
Debris-flow deposits				
Hueyatlaco ravine				
PO1701	17.98	69.20	12.22	0.61
PO02A	19.49	79.05	1.37	0.09
PO02B	5.65	86.42	7.78	0.15
PO02C	4.76	87.52	7.56	0.16
PO05A	6.46	77.81	15.19	0.54
PO05B	2.91	80.49	15.95	0.66
Huitzilac ravine				
PO11	4.25	86.21	9.19	0.34
PO15	0.09	83.54	15.82	0.52
PO17	15.35	77.02	7.41	0.20
PO19	8.49	77.96	13.15	0.38
Xalipilcayatl ravine				
POE04	58.75	36.69	4.25	0.30
POE01	30.77	60.26	8.59	0.36
POE03-upper	62.93	34.45	2.41	0.20
POE03-lower	0.69	88.32	10.63	0.34

References

Almeida, L., Cleef, A. M., Herrera, A., Velazquez, A. and Luna, I.: El zacatonal alpino del Volcán Popocatépetl, México, y su posición en las montañas tropicales de América, Phytocoenologia, 22(3), 391–436, doi:10.1127/phyto/22/1994/391, 1994.

530 Arámbula-Mendoza, R., Valdés-González, C. and Martínez-Bringas, A.: Temporal and spatial variation of the stress state of Popocatépetl Volcano, Mexico, J. Volcanol. Geotherm. Res., 196(3–4), 156–168, doi:10.1016/j.jvolgeores.2010.07.007, 2010.

Bouchon, M., Schultz, C. A. and Toksoz, M. N.: Effect of three-dimensional topography on seismic motion, J. Geophys. Res., 101(B3), 5835–5846, 1996.

535 Camacho, H.: Efectos del temblor sobre el terrano: Chapter V, Tercera Parte, in Memoria Relativa al Terremoto Mexicano del 3 de Enero de 1920, pp. 89–94., 1920.

Capra, L., Poblete, M. A. and Alvarado, R.: The 1997 and 2001 lahars of Popocatépetl volcano (Central Mexico): Textural and sedimentological constraints on their origin and hazards, J. Volcanol. Geotherm. Res., 131(3–4), 351–369, doi:10.1016/S0377-0273(03)00413-X, 2004.

540 Capra, L., Bernal, J. P., Carrasco-Núñez, G. and Roverato, M.: Climatic fluctuations as a significant contributing factor for volcanic collapses. Evidence from Mexico during the Late Pleistocene, Glob. Planet. Change, 100, 194–203,

doi:10.1016/j.gloplacha.2012.10.017, 2013.

Capra, L., Coviello, V., Borselli, L., Márquez-Ramírez, V.-H. and Arámbula-Mendoza, R.: Hydrological control of large hurricane-induced lahars: evidences from rainfall, seismic and video monitoring, Nat. Hazards Earth Syst. Sci., 18(October), 781–794, doi:10.5194/nhess-2017-354, 2018.

Castillo, M., Muñoz-Salinas, E. and Arce, J. L.: Evaluación del sistema erosivo fluvial en el volcán Popocatépetl (México) mediante análisis morfométricos, Bol. la Soc. Geol. Mex., 67(2), 167–183, 2015.

De Cserna, Z., De la Fuente-Duch, M., Palacio-Neto, M., Triay, L., Mitre-Salazar, L. M. and Mota-Palomino, R.: Estructura geológica, gravimétrica y relaciones neotectónicas regionales de la Cuenca de México, Bol. Inst. Geol. UNAM., 104, 71, 1988.

Dadson, S. J., Hovius, N., Chen, H., Dade, W. B., Lin, J. C., Hsu, M. L., Lin, C. W., Horng, M. J., Chen, T. C., Milliman, J. and Stark, C. P.: Earthquake-triggered increase in sediment delivery from an active mountain belt, Geology, 32(8), 733–736, doi:10.1130/G20639.1, 2004.

Davis, L. L. and West, L. R.: Observed effects of topography on ground motion, Bull. Seismol. Soc. Am., 63(1), 283–298, 1973.

Delcamp, A., Roberti, G. and van Wyk de Vries, B.: Water in volcanoes: evolution, storage and rapid release during landslides, Bull. Volcanol., 78(12), doi:10.1007/s00445-016-1082-8, 2016.

Domènech, G., Fan, X., Scaringi, G., van Asch, T. W. J., Xu, Q., Huang, R. and Hales, T. C.: Modelling the role of material depletion, grain coarsening and revegetation in debris flow occurrences after the 2008 Wenchuan earthquake, Eng. Geol., 250(September 2018), 34–44, doi:10.1016/j.enggeo.2019.01.010, 2019.

Espinasa-Perena, R. and Martín-Del Pozzo, A. L.: Morphostratigraphic evolution of popocatépetl volcano, México, Spec. Pap. Geol. Soc. Am., 402(05), 115–137, doi:10.1130/2006.2402(05), 2006.

Fan, X., Scaringi, G., Korup, O., West, A. J., van Westen, C. J., Tanyas, H., Hovius, N., Hales, T. C., Jibson, R. W., Allstadt, K. E., Zhang, L., Evans, S. G., Xu, C., Li, G., Pei, X., Xu, Q. and Huang, R.: Earthquake-Induced Chains of Geologic Hazards: Patterns, Mechanisms, and Impacts, Rev. Geophys., 57(2), 421–503, doi:10.1029/2018RG000626, 2019.

Fan, X., Yunus, A. P., Scaringi, G., Catani, F., Siva Subramanian, S., Xu, Q. and Huang, R.: Rapidly Evolving Controls of Landslides After a Strong Earthquake and Implications for Hazard Assessments, Geophys. Res. Lett., 48(1), 1–12, doi:10.1029/2020GL090509, 2021.

Flores, T.: Efectos geologicos: Chapter IV, Primera Parte, in Memoria del terremoto Mexicano del 3 de enero de 1920, pp. 27–29., 1922.

Furumura, T. and Singh, S. K.: Regional Wave Propagation from Mexican Subduction Zone Earthquakes : The Attenuation Functions for Interplate and Inslab Events, Bull. Seismol. Soc. Am., 92(6), 2110–2125, 2002.

García-Palomo, A., Macías, J. L., Jiménez, A., Tolson, G., Mena, M., Sánchez-Núñez, J. M., Arce, J. L., Layer, P. W., Santoyo, M. Á. and Lermo-Samaniego, J.: NW-SE Pliocene-Quaternary extension in the Apan-Acoculco region, eastern Trans-Mexican Volcanic Belt, J. Volcanol. Geotherm. Res., 349, 240–255, doi:10.1016/j.jvolgeores.2017.11.005, 2018.

García, D., Singh, S. K., Herra, M., Ordaz, M. and Pacheco, J. F.: Inslab Earthquakes of Central Mexico: Peak Ground-Motion Parameters and Response Spectra, Bull. Seismol. Soc. Am., 95(6), 2272–2282, doi:10.1785/0120050072, 2005.

Del Gaudio, V. and Wasowski, J.: Directivity of slope dynamic response to seismic shaking, Geophys. Res. Lett., 34(12), L12301, doi:10.1029/2007GL029842, 2007.

580   Geli, L., Bard, P. and Jullien, B.: THE EFFECT OF TOPOGRAPHY ON EARTHQUAKE GROUND MOTION: A REVIEW AND NEW RESULTS, Bull. Seismol. Soc. Am., 78(1), 42–63, 1988.

Johnson, P. J., Valentine, G. A., Stauffer, P. H., Lowry, C. S., Sonder, I., Pulgarín, B. A., Santacoloma, C. C. and Agudelo, A.: Groundwater drainage from fissures as a source for lahars, Bull. Volcanol., 80(4), doi:10.1007/s00445-018-1214-4, 2018.

585   Julio-Miranda, P., Delgado-Granados, H., Huggel, C. and Kääb, A.: Impact of the eruptive activity on glacier evolution at Popocatépetl Volcano (México) during 1994-2004, J. Volcanol. Geotherm. Res., 170(1–2), 86–98, doi:10.1016/j.jvolgeores.2007.09.011, 2008.

Kameda, J., Kamiya, H., Masumoto, H., Morisaki, T., Hiratsuka, T. and Inaoi, C.: Fluidized landslides triggered by the liquefaction of subsurface volcanic deposits during the 2018 Iburi–Tobu earthquake, Hokkaido, Sci. Rep., 9(1), 1–6,
590   doi:10.1038/s41598-019-48820-y, 2019.

Keefer, D. K.: Landslides caused by earthquakes, GSA Bull., 95(2), 406–421, doi:10.1016/0148-9062(85)92394-0, 1984.

Keefer, D. K., Wartman, J., Navarro Ochoa, C., Rodriguez-Marek, A. and Wieczorek, G. F.: Landslides caused by the M 7.6 Tecomán, Mexico earthquake of January 21, 2003, Eng. Geol., 86(2–3), 183–197, doi:10.1016/j.enggeo.2006.02.017, 2006.

LaHusen, S. R., Duvall, A. R., Booth, A. M., Grant, A., Mishkin, B. A., Montgomery, D. R., Struble, W., Roering, J. J. and
595   Wartman, J.: Rainfall triggers more deep-seated landslides than Cascadia earthquakes in the Oregon Coast Range, USA, Sci. Adv., 6(38), doi:10.1126/sciadv.aba6790, 2020.

Major, J. J., Bertin, D., Pierson, T. C., Amigo, A., Iroumé, A., Ulloa, H. and Castro, J.: Extraordinary sediment delivery and rapid geomorphic response following the 2008–2009 eruption of Chaitén Volcano, Chile, Water Resour. Res., 52, 5075–5094, doi:10.1002/2015WR018250.Received, 2016.

600   Manville, V., Németh, K. and Kano, K.: Source to sink: A review of three decades of progress in the understanding of volcaniclastic processes, deposits, and hazards, Sediment. Geol., 220(3–4), 136–161, doi:10.1016/j.sedgeo.2009.04.022, 2009.

Marc, O., Behling, R., Andermann, C., Turowski, J. M., Illien, L., Roessner, S. and Hovius, N.: Long-term erosion of the Nepal Himalayas by bedrock landsliding: The role of monsoons, earthquakes and giant landslides, Earth Surf. Dyn., 7(1),
605   107–128, doi:10.5194/esurf-7-107-2019, 2019.

Martin Del Pozzo, A. L., Alatorre Ibargüengoitia, M., Arana Salinas, L., Bonasia, R., Capra Pedol, L., Cassata, W., Córdoba, G., Cortés Ramos, J., Delgado Granados, H., Ferrés López, M. D., R., F. Á., García Reynoso, J. A., Gisbert, G., Guerrero López, D. A., Jaimes Viera, M. C., Macías Vázquez, J. L., Nieto Obregón, J., Nieto Torres, A., Paredes Ruiz, P. A., Portocarrero Martínez, J., Renne, P., Rodríguez Espinosa, D. M., Salinas Sánchez, S., Siebe Grabach, C. and Tellez Ugalde,

610 E.: Estudios geológicos y actualización del mapa de peligros del volcán Popocatépetl, Monografías Instituto de Geofísica, UNAM., 2017.

Mcguire, W. J.: Volcano instability: A review of contemporary themes, Geol. Soc. Spec. Publ., 110(110), 1–23, doi:10.1144/GSL.SP.1996.110.01.01, 1996.

Melgar, D., Pérez-Campos, X., Ramirez-Guzman, L., Spica, Z., Espíndola, V. H., Hammond, W. C. and Cabral-Cano, E.:
615 Bend Faulting at the Edge of a Flat Slab: The 2017 Mw7.1 Puebla-Morelos, Mexico Earthquake, Geophys. Res. Lett., 45(6), 2633–2641, doi:10.1002/2017GL076895, 2018.

Meunier, P., Hovius, N. and Haines, J. A.: Topographic site effects and the location of earthquake induced landslides, Earth Planet. Sci. Lett., 275(3–4), 221–232, doi:10.1016/j.epsl.2008.07.020, 2008.

Mondini, A. C.: Measures of spatial autocorrelation changes in multitemporal SAR images for event landslides detection,
620 Remote Sens., 9(6), doi:10.3390/rs9060554, 2017.

Norini, G., Groppelli, G., Lagmay, A. M. F. and Capra, L.: Recent left-oblique slip faulting in the central eastern Trans-Mexican Volcanic Belt : Seismic hazard and geodynamic implications, Tectonics, 25, 1–21, doi:10.1029/2005TC001877, 2006.

Norini, G., Capra, L., Groppelli, G. and Lagmay, A. M. F.: Quaternary sector collapses of Nevado de Toluca volcano
625 (Mexico) governed by regional tectonics and volcanic evolution, Geosphere, 4(5), 854–871, doi:10.1130/GES00165.1, 2008.

Norini, G., Carrasco-Núñez, G., Corbo-Camargo, F., Lermo, J., Rojas, J. H., Castro, C., Bonini, M., Montanari, D., Corti, G., Moratti, G., Piccardi, L., Chavez, G., Zuluaga, M. C., Ramirez, M. and Cedillo, F.: The structural architecture of the Los Humeros volcanic complex and geothermal field, J. Volcanol. Geotherm. Res., 381, 312–329, doi:10.1016/j.jvolgeores.2019.06.010, 2019.

630 Pasquaré, G., Vezzoli, L. and Zanchi, A.: Morphological and structural model of Mexican Volcanic Belt, Geofísica Int., 26.2, 159–175, 1987.

Pearce, A. J. and Watson, A. J.: Effects of earthquake-induced landslides on sediment budget and transport over 50-yr period, Geology, 14, 52–55, 1986.

Reimer, P. J., Austin, W. E. N., Bard, E., Bayliss, A., Blackwell, P. G., Bronk Ramsey, C., Butzin, M., Cheng, H., Edwards,
635 R. L., Friedrich, M., Grootes, P. M., Guilderson, T. P., Hajdas, I., Heaton, T. J., Hogg, A. G., Hughen, K. A., Kromer, B., Manning, S. W., Muscheler, R., Palmer, J. G., Pearson, C., Van Der Plicht, J., Reimer, R. W., Richards, D. A., Scott, E. M., Southon, J. R., Turney, C. S. M., Wacker, L., Adolphi, F., Büntgen, U., Capano, M., Fahrni, S. M., Fogtmann-Schulz, A., Friedrich, R., Köhler, P., Kudsk, S., Miyake, F., Olsen, J., Reinig, F., Sakamoto, M., Sookdeo, A. and Talamo, S.: The IntCal20 Northern Hemisphere Radiocarbon Age Calibration Curve (0-55 cal kBP), Radiocarbon, 62(4), 725–757,
640 doi:10.1017/RDC.2020.41, 2020.

Roberti, G., Friele, P., van Wyk de Vries, B., Ward, B., Clague, J. J., Perotti, L. and Giardino, M.: Rheological evolution of the Mount Meager 2010 debris avalanche, southwestern British Columbia, Geosphere, 13(2), 1–22, doi:10.1130/GES01389.1, 2017.

Roverato, M., Cronin, S., Procter, J. and Capra, L.: Textural features as indicators of debris avalanche transport and

645   emplacement, Taranaki volcano, Bull. Geol. Soc. Am., 127(1–2), 3–18, doi:10.1130/B30946.1, 2015.

Sassa, K.: Landslide disasters triggered by the 2004 Mid-Niigata Prefecture earthquake in Japan, Landslides, 2(2), 135–142, doi:10.1007/s10346-005-0054-4, 2005.

Sato, H. P., Hasegawa, H., Fujiwara, S., Tobita, M., Koarai, M., Une, H. and Iwahashi, J.: Interpretation of landslide distribution triggered by the 2005 Northern Pakistan earthquake using SPOT 5 imagery, Landslides, 4(2), 113–122,

650   doi:10.1007/s10346-006-0069-5, 2007.

Schulz, W. H., Galloway, S. L. and Higgins, J. D.: Evidence for earthquake triggering of large landslides in coastal Oregon, USA, Geomorphology, 141–142, 88–98, doi:10.1016/j.geomorph.2011.12.026, 2012.

Schuster, R. L., Nieto, A. S., O'Rourke, T. D., Crespo, E. and Plaza-Nieto, G.: Mass wasting triggered by the 5 March 1987 Ecuador earthquakes, Eng. Geol., 42(1), 1–23, doi:10.1016/0013-7952(95)00024-0, 1996.

655   Scott, K. M., Macias, J. L., Naranj, J. A., Rodriguez, S. and McGeehin, J. P.: Catastrophic debris flows transformed from landslides in volcanic terrains: mobility, hazard assessment and mitigation strategies, USGS Professional Paper 1630., 2001.

Serey, A., Piñero-Feliciangeli, L., Sepúlveda, S. A., Poblete, F., Petley, D. N. and Murphy, W.: Landslides induced by the 2010 Chile megathrust earthquake: a comprehensive inventory and correlations with geological and seismic factors, Landslides, (August 2018), 1153–1165, doi:10.1007/s10346-019-01150-6, 2019.

660   Shapiro, N. M., Singh, S. K., Iglesias-Mendoza, A., Cruz-Atienza, V. M. and Pacheco, J. F.: Evidence of low Q below Popocatpetl volcano, and its implication to seismic hazard in Mexico City, Geophys. Res. Lett., 27(17), 2753–2756, doi:10.1029/1999GL011232, 2000.

Siebe, C. and Macías, J. L.: Volcanic hazards in the Mexico City metropolitan area from eruptions at Popocatépetl, Nevado de Toluca, and Jocotitlán stratovolcanoes and monogenetic scoria cones in the Sierra Chichinautzin Volcanic Field., 2006.

665   Siebe, C., Abrams, M., Macías, J. L. and Obenholzner, J.: Repeated volcanic disasters in Prehispanic time at Popocatépetl, central Mexico: Past key to the future?, Geology, 24(5), 399–402, doi:10.1130/0091-7613(1996)024<0399:RVDIPT>2.3.CO;2, 1996.

Siebe, C., Salinas, S., Arana-Salinas, L., Macías, J. L., Gardner, J. and Bonasia, R.: The ~ 23,500 y 14 C BP White Pumice Plinian eruption and associated debris avalanche and Tochimilco lava flow of Popocatépetl volcano, México, J. Volcanol.

670   Geotherm. Res., 333–334, 66–95, doi:10.1016/j.jvolgeores.2017.01.011, 2017.

Siebert, L.: Landslides resulting from structural failure of volcanoes, Rev. Eng. Geol., 15, 209–235, doi:10.1130/REG15-p209, 2002.

Singh, A.: Review article digital change detection techniques using remotely-sensed data, Int. J. Remote Sens., 10(6), 689–1003, doi:10.1007/BF02197115, 1989.

675   Singh, S. K., Reinoso, E., Arroyo, D., Ordaz, M., Cruz-Atienza, V., Pérez-Campos, X., Iglesias, A. and Hjörleifsdóttir, V.: Deadly Intraslab Mexico Earthquake of 19 September 2017 (Mw 7.1): Ground Motion and Damage Pattern in Mexico City, Seismol. Res. Lett., 89(6), 2193–2203, doi:10.1785/0220180159, 2018.

Von Specht, S., Ozturk, U., Veh, G., Cotton, F. and Korup, O.: Effects of finite source rupture on landslide triggering: The 2016 Mw 7.1 Kumamoto earthquake, Solid Earth, 10(2), 463–486, doi:10.5194/se-10-463-2019, 2019.

680   Tanarro, L. M., Andrés, N., Zamorano, J. J., Palacios, D. and Renschler, C. S.: Geomorphological evolution of a fluvial channel after primary lahar deposition: Huiloac Gorge, Popocatépetl volcano (Mexico), Geomorphology, 122(1–2), 178–190, doi:10.1016/j.geomorph.2010.06.013, 2010.

Vázquez-Selem, L. and Heine, K.: Late Quaternary Glaciation in Mexico, in Developments in Quaternary Science, vol. 15, pp. 849–861., 2011.

685   Wang, F., Fan, X., Yunus, A. P., Siva Subramanian, S., Alonso-Rodriguez, A., Dai, L., Xu, Q. and Huang, R.: Coseismic landslides triggered by the 2018 Hokkaido, Japan (Mw 6.6), earthquake: spatial distribution, controlling factors, and possible failure mechanism, Landslides, 16(8), 1551–1566, doi:10.1007/s10346-019-01187-7, 2019.

Wartman, J., Dunham, L., Tiwari, B. and Pradel, D.: Landslides in eastern Honshu induced by the 2011 Off the Pacific Coast of Tohoku earthquake, Bull. Seismol. Soc. Am., 103(2 B), 1503–1521, doi:10.1785/0120120128, 2013.

690   Xu, C. and Xu, X.: Statistical analysis of landslides caused by the Mw 6.9 Yushu, China, earthquake of April 14, 2010, Nat. Hazards, 72, 871–893, doi:10.1007/s11069-014-1038-2, 2014.